Quaternary Science Reviews ∎ (∎∎∎∎) ∎∎∎–∎∎∎

Sea-surface temperature and sea ice distribution of the Southern Ocean at the EPILOG Last Glacial Maximum—a circum-Antarctic view based on siliceous microfossil records ☆

Rainer Gersonde[a,*], Xavier Crosta[b], Andrea Abelmann[a], Leanne Armand[c]

[a]Alfred Wegener Institute for Polar and Marine Research, Bremerhaven, Germany
[b]DGO, UMR-CNRS 5805 EPOC, Université de Bordeaux I, Talence cedex, France
[c]School of Earth Sciences, University of Tasmania, Hobart, Tasmania, Australia

Received 8 January 2004; accepted 10 July 2004

Abstract

Based on the quantitative study of diatoms and radiolarians, summer sea-surface temperature (SSST) and sea ice distribution were estimated from 107 sediment core localities in the Atlantic, Indian and Pacific sectors of the Southern Ocean to reconstruct the last glacial environment at the EPILOG (19.5–16.0 ka or 23 000–19 000 cal yr. B.P.) time-slice. The statistical methods applied include the Imbrie and Kipp Method, the Modern Analog Technique and the General Additive Model. Summer SSTs reveal greater surface-water cooling than reconstructed by CLIMAP (Geol. Soc. Am. Map Chart. Ser. MC-36 (1981) 1), reaching a maximum (4–5 °C) in the present Subantarctic Zone of the Atlantic and Indian sector. The reconstruction of maximum winter sea ice (WSI) extent is in accordance with CLIMAP, showing an expansion of the WSI field by around 100% compared to the present. Although only limited information is available, the data clearly show that CLIMAP strongly overestimated the glacial summer sea ice extent. As a result of the northward expansion of Antarctic cold waters by 5–10° in latitude and a relatively small displacement of the Subtropical Front, thermal gradients were steepened during the last glacial in the northern zone of the Southern Ocean. Such reconstruction may, however, be inapposite for the Pacific sector. The few data available indicate reduced cooling in the southern Pacific and give suggestion for a non-uniform cooling of the glacial Southern Ocean.

This study is part of MARGO, a multiproxy approach for the reconstruction of the glacial ocean surface.

1. Introduction

About 25 years ago Hays et al. (1976) published their pioneering study on the Southern Ocean surface water temperature and sea ice extent during the Last Glacial Maximum (LGM), based on 34 cores from the Atlantic and the western Indian sectors of the Southern Ocean. Austral summer (February) and winter (August) sea-surface temperatures (SST) were estimated using the Imbrie and Kipp (1971) transfer function technique, applying a radiolarian-based paleoecological equation from Lozano and Hays (1976). The standard error was 1.5 °C for the summer and 1.4 °C for the winter estimates. The LGM sea ice boundary was reconstructed by mapping the lithological boundary between diatom-rich and diatom-poor sediments. Because in most cores no continuous calcareous microfossil records were preserved allowing the establishment of an oxygen isotope record, the definition of the LGM level, set at 18 ka, was based on the abundance pattern of the radiolarian *Cycladophora davisiana*. The pattern was calibrated in four cores recovered from the Subantarctic and Subtropical Zone with the oxygen isotope stratigraphy obtained from three planktic and one benthic

☆This paper is dedicated to the diatom paleoceanographer Dr. Jean-Jacques Pichon who died on September 9, 2003 in a tragic accident.

*Corresponding author. Tel.: +49-471-4831-203; fax: +49-471-4831-1923.
E-mail address: rgersonde@awi-bremerhaven.de (R. Gersonde).

0277-3791/$ - see front matter © 2004 Elsevier Ltd. All rights reserved.
doi:10.1016/j.quascirev.2004.07.015

foraminiferal records and a few ^{14}C measurements, all Holocene in age. The stratigraphic determination of the LGM and the SST reconstruction proposed by Hays et al. (1976) was used by Climate Long-range Investigation, Mapping, and Prediction (CLIMAP) (1976, 1981) to estimate circum-Antarctic SST and sea ice distribution as a part of the first global ocean LGM reconstruction. CLIMAP (1976, 1981) placed the austral winter and summer sea ice edge at the faunally identified 0 °C winter and summer isotherm, respectively. Later, Cooke and Hays (1982) presented a revised estimation of the LGM summer and winter sea ice (WSI) extent, considering additional parameters, such as changes in sedimentation rates and the quantification of ice-rafted debris. Burckle et al. (1982) and Burckle (1983) supported this approach, but proposed that the lithological boundary between silty diatomaceous clay and diatom ooze identifies the spring/summer sea ice limits. Alternative attempts to reconstruct past sea ice cover rely on the distribution of diatom sea ice indicators preserved in the sediment record as reviewed in Armand and Leventer (2003). Crosta et al. (1998a, b) were the first to use the Modern Analog Technique (MAT), established by Hutson (1980), for quantitative reconstruction of circum-Antarctic sea ice distribution (months/year) at the LGM levels defined by CLIMAP (1976, 1981). Most recently, Gersonde et al. (2003a) presented a new LGM reconstruction of the Atlantic and western Indian sectors of the Southern Ocean applying IKM or MAT on siliceous (diatoms, radiolarians) and calcareous (planktic foraminifers) microfossil assemblages for SST estimation, and diatom indicator species for the identification of the sea ice extent. This multi-proxy approach was part of "Glacial Atlantic Ocean Mapping" (GLAMAP-2000), an initiative for the reconstruction of the Atlantics SST and sea ice at well-defined LGM time slices (Sarnthein et al., 2003).

Here we present a new circum-Antarctic view of the Southern Oceans SST and sea ice fields during the LGM. This represents a "state-of-the-art" compilation of yet published and new data sets of SST and sea ice estimates from a total of 107 Southern Ocean sediment cores generated from the siliceous microfossil record (diatoms, radiolarians) (Fig. 1). Our compilation is part of the international "Multiproxy Approach for the Reconstruction of the Glacial Ocean Surface"(MARGO) initiative, started in 2002. The data have been assembled following the rules agreed upon by the MARGO scientific community (Kucera et al., 2004). This includes a well-defined quality control for the selection of used sample material and quality ranking of the obtained data. As suggested by MARGO, we follow the LGM time slice definition (19.5–16.0 ka, equal to 23 000–19 000 cal yr B.P.) proposed by the international "Environment Processes of the Ice Age: Land, Ocean, Glaciers" (EPILOG) working group (Mix et al., 2001). Our Southern Ocean EPILOG-LGM (E-LGM) compilation represents a major step to describe and understand environmental conditions and processes in a part of the World Ocean that acts as a major player in global climate change through feedback mechanisms driven by changes in albedo, ocean/atmosphere exchange rates, physical parameters of ocean surface waters, water mass structure and formation, and biological productivity. Of crucial interest is the reconstruction of sea ice and its seasonal variability. Sea ice represents a fast reacting climate amplifier, causing enhanced variability during glacial intervals, as a result of its impact on water mass production and circulation, as well as air-sea gas and energy exchange (Stephens and Keeling, 2000; Keeling and Stephens, 2001). Sea ice also impacts the Earths albedo and it gears latitudinal thermal gradients and storminess and thus, involves the lofting of dust, micronutrient iron and sea salt into the atmosphere (Broecker, 2001). Amalgamated with the results obtained from other ocean basins within MARGO, the presented reconstructions of summer and winter conditions will help to provide information on climate end-member conditions at the global scale required to test climate models and to increase their fidelity to simulate future climate change. Our study also identifies current deficiencies in the methods used for reconstruction of past Southern Ocean conditions, as acknowledging existing gaps of information.

2. Material, methods, age determination and quality control

2.1. Sample preparation and counting

Preparation of sediment samples for light-microscopic investigations was done according to various techniques. Diatom samples collected during R.V. *Polarstern* cruises (PS indexed sample sites) were cleaned according to the method described by Gersonde and Zielinski (2000) for diatoms. All other diatom samples were treated using a method adapted from Schrader and Gersonde (1978) and Pichon et al. (1992a). Radiolarian samples have been cleaned according to the method described by Abelmann (1988) and Abelmann et al. (1999).

Preparation of permanent mounts for light microscopic investigation was completed according to Gersonde and Zielinski (2000) for diatom slides, and according to Abelmann et al. (1999) for radiolarian slides.

Diatom counts followed the conventions of Schrader and Gersonde (1978) and Laws (1983). A minimum of 300 diatom valves or radiolarian skeletons (in average around 400) was counted in each sample using high quality photomicroscopes (Leitz, Olympus, Zeiss) at a

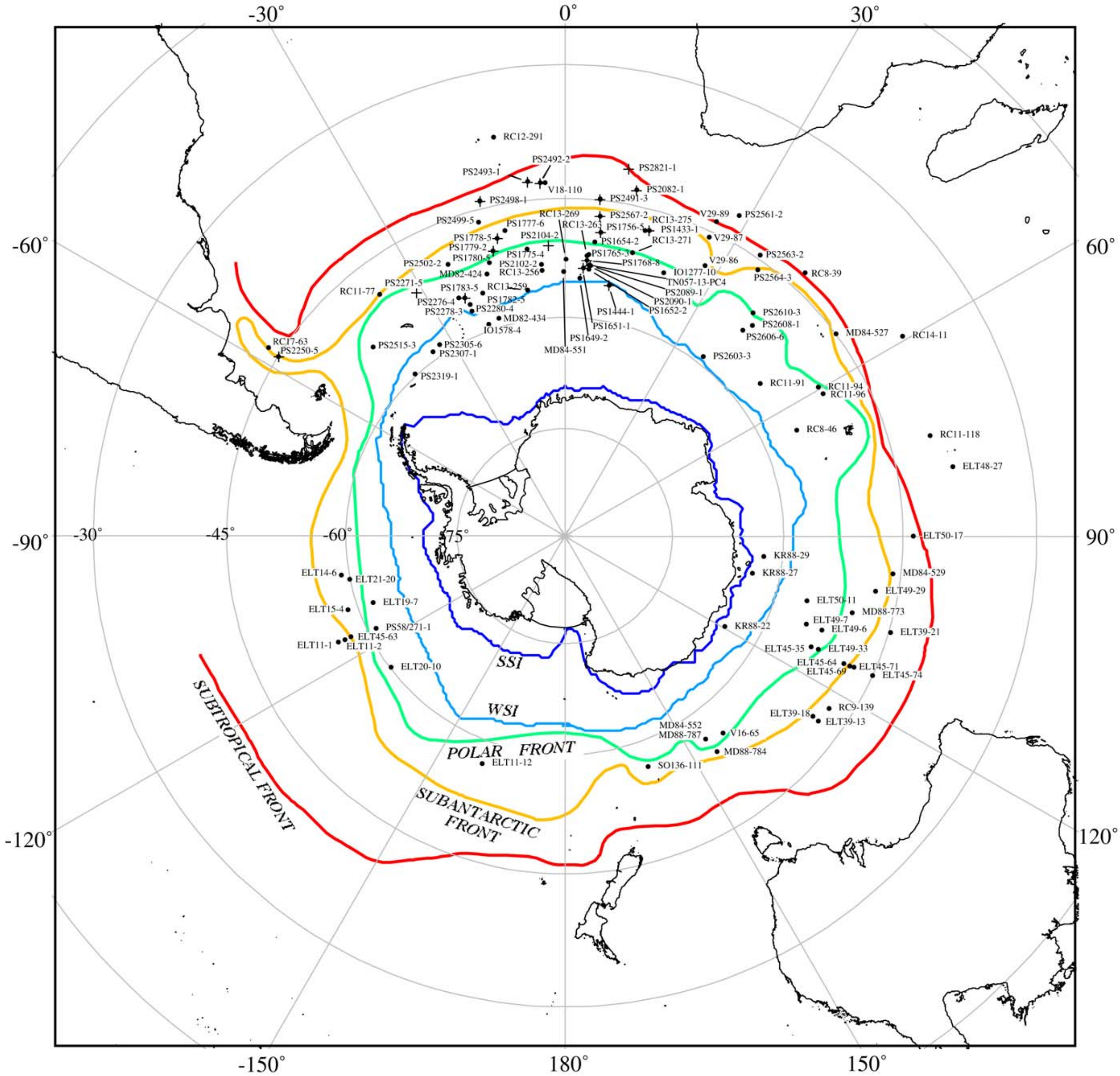

Fig. 1. Distribution of cores used for E-LGM reconstruction. Closed points indicate locations with diatom-based reconstruction, crosses indicate location with radiolarian-based reconstruction. For core location information see Table 3. Location of oceanic fronts according to Belkin and Gordon (1996). The sea ice distribution is from data of Comiso (2003), WSI indicates > 15% September sea ice concentration average (1979–1999), summer sea ice (SSI) > 15% February concentration average (1979–1999).

magnification of 1000 × for diatom counts and of 250 × or 400 × for radiolarian counts.

2.2. Reconstruction techniques and reference data sets

Statistical methods used for the estimation of SSTs and sea ice include the classical Imbrie and Kipp Method (IKM; Imbrie and Kipp, 1971), the MAT (Hutson, 1980) and the recently proposed Generalized Additive Model (GAM; Hastie and Tibshirani, 1990). The basic assumption of these techniques is that the modern spatial variability of microfossil assemblages in surface sediment samples deposited at known environmental conditions serves as a proxy for past environmental variability documented down-core.

By means of factor analysis, the IKM resolves microfossil assemblages preserved in surface sediment samples. The resulting varimax factors are calibrated in terms of hydrographic parameters of the surface waters, such as temperature, by using a stepwise multiple regression analysis, which is then applied to down-core assemblages to estimate past hydrographic parameters. For further reading on the IKM, we refer to Imbrie and Kipp (1971), Maynard (1976), Jöreskog et al. (1976), Malmgren and Haq (1982), Le (1992), and Le and Shackleton (1994).

IKM was used for E-LGM SST reconstruction at 45 sites in the Atlantic and eastern Indian sector of the Southern Ocean (Gersonde et al., 2003a) and at one site in the eastern Pacific sector (Wittling and Gersonde, unpublished data) applying a regional diatom and/or radiolarian reference data set. According to sensitivity tests by Le (1992), regional data sets exhibit better statistical results using the IKM than other techniques. For this reason we carefully selected 93 surface sediment samples from a total of 218 samples in the Atlantic and Indian Ocean sectors (Zielinski and Gersonde, 1997) (Fig. 2, Table 1). This diatom reference data set contains 29 species or species groups. Many of the selected surface samples have been recovered with a multicorer (MC) device, allowing undisturbed sampling of the sediment surface (Table 1). For SST estimates a logarithmic ranking of the diatom abundance data was applied in order to compensate the dominance of one diatom species, *Fragilariopsis kerguelensis*. The documentation of the diatom reference data set and the

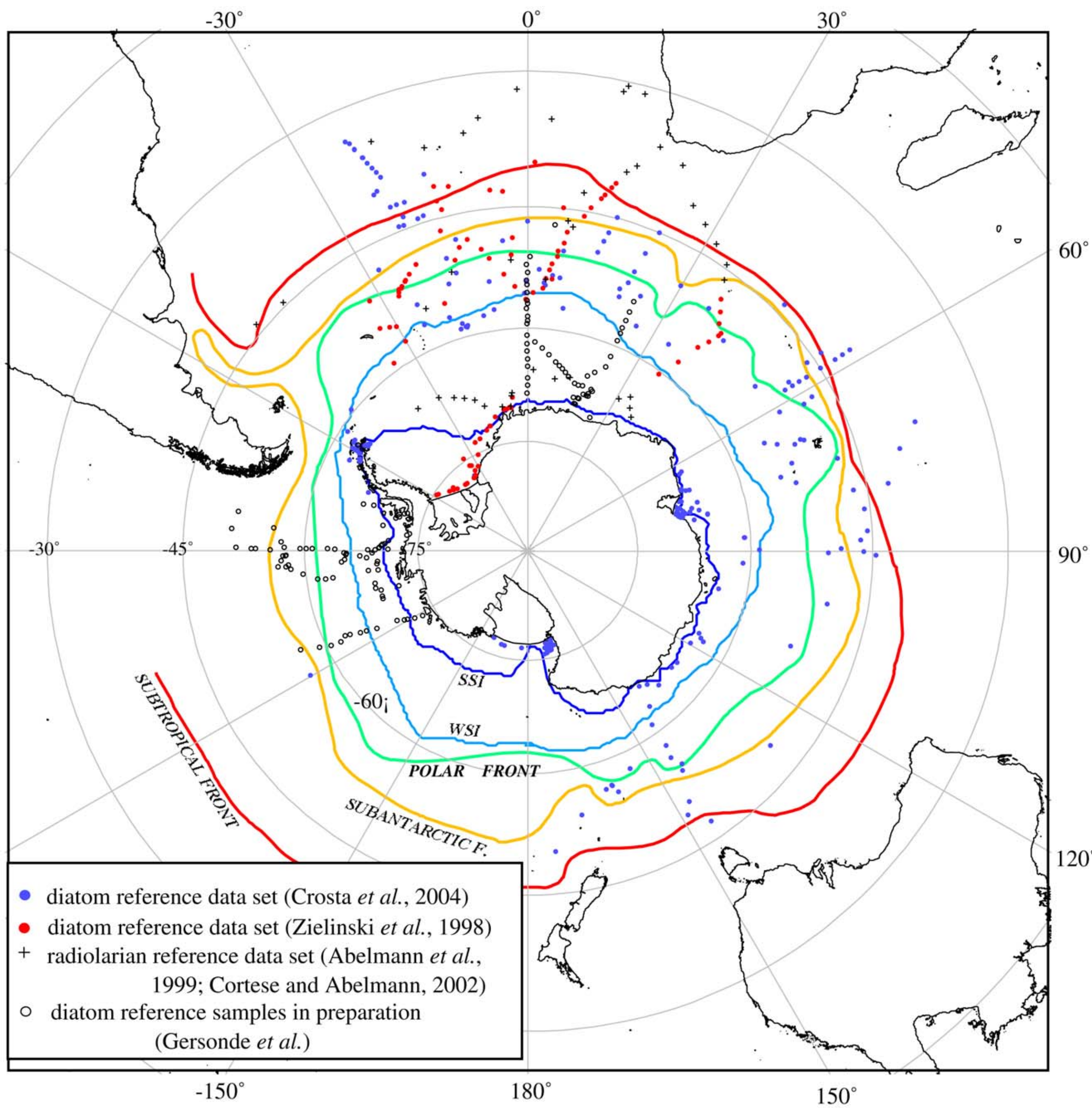

Fig. 2. Distribution of diatom and radiolarian reference samples in the Southern Ocean. For sample location information see Table 1.

Table 1
Compilation of reference surface sediment samples used for diatom (D) and radiolarian (R) based estimation of summer SST and sea-ice (see also Fig. 2 for map)

Core	Longitude	Latitude	Water depth (m)	Coring device	Sampling level	Strat. quality	Fossil group	Use	Ref.
AA93-7/105GR	−66.56	62.74	1882	BC	Top	4	D	MAT/GAM-SST/SI	1
AA93-7/106GR	−66.87	63.16	434	BC	Top	4	D	MAT/GAM-SST/SI	1
AA93-7/12GR	−68.7	77.51	707	BC	Top	4	D	MAT/GAM-SST/SI	1
AA93-7/13GR	−68.67	77.27	538	BC	Top	4	D	MAT/GAM-SST/SI	1
AA93-7/14GR	−68.91	76.9	700	BC	Top	4	D	MAT/GAM-SST/SI	1
AA93-7/15GR	−68.82	77.17	760	BC	Top	4	D	MAT/GAM-SST/SI	1
AA93-7/17GR	−68.78	76.8	798	BC	Top	4	D	MAT/GAM-SST/SI	1
AA93-7/18GR	−68.71	76.74	820	BC	Top	4	D	MAT/GAM-SST/SI	1
AA93-7/19GR	−68.65	76.72	775	BC	Top	4	D	MAT/GAM-SST/SI	1
AA93-7/21GR	−68.01	76.55	460	BC	Top	4	D	MAT/GAM-SST/SI	1
AA93-7/23GR	−67.35	76.59	318	BC	Top	4	D	MAT/GAM-SST/SI	1
AA93-7/24GR	−66.97	79.26	330	BC	Top	4	D	MAT/GAM-SST/SI	1
AA93-7/37GR	−68.96	75.19	775	BC	Top	4	D	MAT/GAM-SST/SI	1
AA93-7/38GR	−68.61	74.52	667	BC	Top	4	D	MAT/GAM-SST/SI	1
AA93-7/39GR	−68.55	74.42	775	BC	Top	4	D	MAT/GAM-SST/SI	1
AA93-7/41GR	−68.94	73.57	792	BC	Top	4	D	MAT/GAM-SST/SI	1
AA93-7/42GR	−68.18	75.87	695	BC	Top	4	D	MAT/GAM-SST/SI	1
AA93-7/43GR	−69.23	76.1	548	BC	Top	4	D	MAT/GAM-SST/SI	1
AA93-7/59GR	−68.41	72.01	509	BC	Top	4	D	MAT/GAM-SST/SI	1
AA93-7/60GR	−68.1	72.25	788	BC	Top	4	D	MAT/GAM-SST/SI	1
AA93-7/73GR	−66.56	69.4	1435	BC	Top	4	D	MAT/GAM-SST/SI	1
AA93-7/78GR	−67.51	68.2	460	BC	Top	4	D	MAT/GAM-SST/SI	1
AA93-7/9GR	−68.43	77.81	173	BC	Top	4	D	MAT/GAM-SST/SI	1
AA93-7/GR158	−68.92	76.62	700	BC	Top	4	D	MAT/GAM-SST/SI	1
DF86-119TC	−66.95	−69.86	600	TRIG	Top	4	D	MAT/GAM-SST/SI	1
DFBC83-10II	−76.95	166.33	878	BC	Top	4	D	MAT/GAM-SST/SI	1
DFBC83-19III	−77.3	−158.72	677	BC	Top	4	D	MAT/GAM-SST/SI	1
DFBC83-1II	−76.17	168.96	540	BC	Top	4	D	MAT/GAM-SST/SI	1
DFBC83-1III	−77.17	169.12	930	BC	Top	4	D	MAT/GAM-SST/SI	1
DFBC83-20II	−76.95	166.68	750	BC	Top	4	D	MAT/GAM-SST/SI	1
DFBC83-21II	−76.69	167.82	768	BC	Top	4	D	MAT/GAM-SST/SI	1
DFBC83-23II	−76.52	170.09	860	BC	Top	4	D	MAT/GAM-SST/SI	1
DFBC83-27II	−75.7	170.65	322	BC	Top	4	D	MAT/GAM-SST/SI	1
DFBC83-28II	−75.85	169.3	485	BC	Top	4	D	MAT/GAM-SST/SI	1
DFBC83-29II	−76.02	167.2	622	BC	Top	4	D	MAT/GAM-SST/SI	1
DFBC83-2II	−76.62	164.35	540	BC	Top	4	D	MAT/GAM-SST/SI	1
DFBC83-30II	−76.09	166.7	668	BC	Top	4	D	MAT/GAM-SST/SI	1
DFBC83-40II	−76.35	167.2	732	BC	Top	4	D	MAT/GAM-SST/SI	1
DFBC83-41III	−76.67	−164.02	516	BC	Top	4	D	MAT/GAM-SST/SI	1
DFBC83-42III	−76.63	−166.05	420	BC	Top	4	D	MAT/GAM-SST/SI	1
DFBC83-43III	−76.72	−176.32	541	BC	Top	4	D	MAT/GAM-SST/SI	1
DFBC83-5II	−76.5	166	640	BC	Top	4	D	MAT/GAM-SST/SI	1
DFBC83-6II	−77.5	165.8	823	BC	Top	4	D	MAT/GAM-SST/SI	1
DFBC83-7II	−77.35	165.88	880	BC	Top	4	D	MAT/GAM-SST/SI	1
DFBC83-8II	−77.17	165.8	871	BC	Top	4	D	MAT/GAM-SST/SI	1
DFBC83-9II	−77.09	166.32	915	BC	Top	4	D	MAT/GAM-SST/SI	1
ELT33-21	−56.54	−119.8	2240	TRIG	1–2	5	D	MAT/GAM-SST/SI	1
ELT36-33	−57.77	154.88	1877	TRIG	Top	4	D	MAT/GAM-SST/SI	1
ELT36-38	−56.47	161.76	2258	TRIG	3–4	5	D	MAT/GAM-SST/SI	1
GC33	−67.68	68.5	320	GRAV	Top	2	D	MAT/GAM-SST/SI	1
GC5	−67.05	69.09	376	GRAV	Top	2	D	MAT/GAM-SST/SI	1
GeoB2004-1	−30.87	14.34	2569	MC	0–0.5	4	R	IKM-SST	4
GeoB2007-1	−30.44	12.16	3906	BC	0–1	4	R	IKM-SST	4
GeoB2008-1	−31.1	11.72	4312	BC	0–1	4	R	IKM-SST	4
GeoB2016-3	−31.91	−1.3	3385	MC	0–0.5	4	R	IKM-SST	4
GeoB2018-1	−34.66	−6.56	4241	MC	0–0.5	4	R	IKM-SST	4
GeoB2019-2	−36.05	−8.77	3825	MC	0–0.5	4	R	IKM-SST	4
GeoB2021-4	−36.83	−14.4	3575	MC	0–0.5	4	R	IKM-SST	4
GeoB2022-3	−34.44	−20.89	4025	MC	0–0.5	4	R	IKM-SST	4
GeoB6402-9	−39.75	−22.76	3878	BC	Top	4	D	MAT/GAM-SST/SI	1
GeoB6403-4	−40.01	−23.36	4226	MC	Top	4	D	MAT/GAM-SST/SI	1

Table 1 (*continued*)

Core	Longitude	Latitude	Water depth (m)	Coring device	Sampling level	Strat. quality	Fossil group	Use	Ref.
GeoB6405-8	−42.01	−21.85	3862	MC	Top	4	D	MAT/GAM-SST/SI	1
GeoB6406-1	−42.01	−20.79	3514	MC	Top	4	D	MAT/GAM-SST/SI	1
GeoB6407-2	−42.04	−19.5	3384	MC	Top	4	D	MAT/GAM-SST/SI	1
GeoB6408-3	−43.61	−20.45	3797	BC	Top	4	D	MAT/GAM-SST/SI	1
GeoB6409-3	−44.51	−21.72	4269	BC	Top	4	D	MAT/GAM-SST/SI	1
GeoB6410-1	−44.52	−20.9	4038	MC	Top	4	D	MAT/GAM-SST/SI	1
GeoB6411-4	−44.37	−18.35	3893	BC	Top	4	D	MAT/GAM-SST/SI	1
GeoB6413-4	−44.21	−17.34	3768	BC	Top	4	D	MAT/GAM-SST/SI	1
GeoB6418-3	−38.43	−21.53	4126	BC	Top	4	D	MAT/GAM-SST/SI	1
GeoB6419-1	−37.78	−21.83	3568	BC	Top	4	D	MAT/GAM-SST/SI	1
GeoB6420-2	−37.12	−22.16	3998	BC	Top	4	D	MAT/GAM-SST/SI	1
GeoB6421-1	−36.45	−22.47	4216	BC	Top	4	D	MAT/GAM-SST/SI	1
GeoB6422-5	−35.71	−22.73	3972	BC	Top	4	D	MAT/GAM-SST/SI	1
GeoB6424-2	−34.61	−23.28	3820	BC	Top	4	D	MAT/GAM-SST/SI	1
GeoB6425-1	−33.83	−23.59	4352	BC	Top	4	D	MAT/GAM-SST/SI	1
GeoB6426-2	−33.5	−24.02	4381	MC	Top	4	D	MAT/GAM-SST/SI	1
IO1176-55	−53.39	6.66	2926	KULL	Top	4	D	MAT/GAM-SST/SI	1
IO1176-65	−57.21	8.21	5483	KULL	Top	4	D	MAT/GAM-SST/SI	1
IO1176-82	−49.52	13.2	4100	KULL	Top	4	D	MAT/GAM-SST/SI	1
IO1176-86	−48.03	13.82	4338	KULL	Top	4	D	MAT/GAM-SST/SI	1
IO1176-88	−46.95	14.31	5106	KULL	Top	4	D	MAT/GAM-SST/SI	1
IO1176-91	−44.94	15.05	4649	KULL	Top	4	D	MAT/GAM-SST/SI	1
IO1277-10	−52.02	20.47	2740	KULL	Top	4	D	MAT/GAM-SST/SI	1
IO1277-12	−54.01	19.79	3178	KULL	Top	4	D	MAT/GAM-SST/SI	1
IO1277-2	−45.03	22.45	4806	KULL	Top	4	D	MAT/GAM-SST/SI	1
IO1277-4	−47.98	21.58	3150	KULL	Top	4	D	MAT/GAM-SST/SI	1
IO1277-8	−50.54	20.89	4492	KULL	Top	4	D	MAT/GAM-SST/SI	1
IO1678-112	−48.15	−27.98	3250	KULL	Top	4	D	MAT/GAM-SST/SI	1
IO1678-64	−54.01	−24.19	4515	KULL	Top	4	D	MAT/GAM-SST/SI	1
IO1678-80	−47.95	−13.03	3120	KULL	Top	4	D	MAT/GAM-SST/SI	1
IO1678-84	−51.96	−14.42	3952	KULL	Top	4	D	MAT/GAM-SST/SI	1
IO1678-89	−57.06	−18.54	4285	KULL	Top	4	D	MAT/GAM-SST/SI	1
KR 88-04	−49.93	100.08	3350	BC	Top	4	D	MAT/GAM-SST/SI	1
KR87-06	−63.05	−63.05	630	BC	Top	4	D	MAT/GAM-SST/SI	1
KR87-07	−62.35	−57.96	2810	BC	Top	4	D	MAT/GAM-SST/SI	1
KR87-08	−60.92	−56.44	2150	BC	Top	4	D	MAT/GAM-SST/SI	1
KR87-10	−59.65	−51.27	2820	BC	Top	4	D	MAT/GAM-SST/SI	1
KR88-01	−46.69	79.48	2925	BC	Top	4	D	MAT/GAM-SST/SI	1
KR88-02	−45.75	82.94	3480	BC	Top	4	D	MAT/GAM-SST/SI	1
KR88-03	−46.07	90.11	3400	MC	Top	4	D	MAT/GAM-SST/SI	1
KR88-05	−52.95	109.92	3510	BC	Top	4	D	MAT/GAM-SST/SI	1
KR88-06	−49.02	128.78	3850	BC	Top	4	D	MAT/GAM-SST/SI	1
KR88-07	−47.15	145.79	2890	BC	Top	4	D	MAT/GAM-SST/SI	1
KR88-08	−49.26	148.8	3885	BC	Top	4	D	MAT/GAM-SST/SI	1
KR88-09	−50.59	147.16	4350	BC	Top	4	D	MAT/GAM-SST/SI	1
KR88-10	−54.19	144.8	2785	BC	Top	4	D	MAT/GAM-SST/SI	1
KR88-11	−54.92	144.07	2880	BC	Top	4	D	MAT/GAM-SST/SI	1
KR88-12	−56.4	145.29	3020	BC	Top	4	D	MAT/GAM-SST/SI	1
KR88-13	−57.95	144.58	3740	BC	Top	4	D	MAT/GAM-SST/SI	1
KR88-14	−61.23	144.44	4200	BC	Top	4	D	MAT/GAM-SST/SI	1
KR88-15	−63.31	141.93	3880	BC	Top	4	D	MAT/GAM-SST/SI	1
KR88-17	−66.2	140.5	180	BC	Top	4	D	MAT/GAM-SST/SI	1
KR88-18	−65.75	138.2	615	BC	Top	4	D	MAT/GAM-SST/SI	1
KR88-19	−64.57	135.63	2930	BC	Top	4	D	MAT/GAM-SST/SI	1
KR88-20	−64.94	129	1670	BC	Top	4	D	MAT/GAM-SST/SI	1
KR88-21	−64.82	126.72	2250	BC	Top	4	D	MAT/GAM-SST/SI	1
KR88-22	−64.67	119.5	3140	BC	Top	4	D	MAT/GAM-SST/SI	1
KR88-23	−63.3	117.26	3292	BC	Top	4	D	MAT/GAM-SST/SI	1
KR88-24	−63.75	116.75	2600	BC	Top	4	D	MAT/GAM-SST/SI	1
KR88-25	−64.3	115.7	2232	BC	Top	4	D	MAT/GAM-SST/SI	1
KR88-27	−63.65	101.15	1210	BC	Top	4	D	MAT/GAM-SST/SI	1
KR88-30	−61	93.2	4300	BC	Top	4	D	MAT/GAM-SST/SI	1
KR88-31	−59	89.6	4595	BC	Top	4	D	MAT/GAM-SST/SI	1

Table 1 (*continued*)

Core	Longitude	Latitude	Water depth (m)	Coring device	Sampling level	Strat. quality	Fossil group	Use	Ref.
KTB01	−49.12	57.02	1235	MC	Top	4	D	MAT/GAM-SST/SI	1
KTB08	−51.98	61.11	4710	MC	Top	4	D	MAT/GAM-SST/SI	1
KTB12	−49	57.98	4390	MC	Top	4	D	MAT/GAM-SST/SI	1
KTB14	−50	57.98	4610	MC	Top	4	D	MAT/GAM-SST/SI	1
KTB18	−48	57.98	4245	MC	Top	4	D	MAT/GAM-SST/SI	1
KTB20	−47	58.02	4550	MC	Top	4	D	MAT/GAM-SST/SI	1
KTB21	−45.96	55.98	4195	MC	Top	4	D	MAT/GAM-SST/SI	1
KTB22	−45.98	55.98	4260	MC	Top	4	D	MAT/GAM-SST/SI	1
KTB25	−45.02	57.94	4680	BC	Top	4	D	MAT/GAM-SST/SI	1
KTB26	−43.97	55.95	4527	MC	Top	4	D	MAT/GAM-SST/SI	1
KTB29	−43	58.02	4765	MC	Top	4	D	MAT/GAM-SST/SI	1
KTB31	−40.98	57.98	5077	MC	Top	4	D	MAT/GAM-SST/SI	1
KTB34	−41.98	58.02	4800	MC	Top	4	D	MAT/GAM-SST/SI	1
MD24-KK02	−54.22	3.52	1522	KULL	Top	4	D	MAT/GAM-SST/SI	1
MD24-KK32	−54.5	3.81	2020	KULL	Top	4	D	MAT/GAM-SST/SI	1
MD24-KK35	−53.11	19.41	2725	KULL	Top	4	D	MAT/GAM-SST/SI	1
MD24-KK37	−52.97	23.77	2905	KULL	Top	4	D	MAT/GAM-SST/SI	1
MD24-KK63	−51.93	42.88	2550	KULL	Top	4	D	MAT/GAM-SST/SI	1
MD80-301	−54	66.83	3750	KULL	Top	4	D	MAT/GAM-SST/SI	1
MD80-304	−51.07	67.73	1950	KULL	Top	4	D	MAT/GAM-SST/SI	1
MD82-422	−52.56	2.24	3750	KULL	Top	4	D	MAT/GAM-SST/SI	1
MD82-424	−54.09	−0.34	2350	KULL	Top	4	D	MAT/GAM-SST/SI	1
MD82-425	−55.58	−0.72	1940	KULL	Top	4	D	MAT/GAM-SST/SI	1
MD82-428	−57.32	−7.98	3750	KULL	Top	4	D	MAT/GAM-SST/SI	1
MD82-430	−57.87	−10.68	3863	KULL	Top	4	D	MAT/GAM-SST/SI	1
MD82-432	−58.64	−14.93	4150	KULL	Top	4	D	MAT/GAM-SST/SI	1
MD82-433	−58.88	−15.2	4750	KULL	Top	4	D	MAT/GAM-SST/SI	1
MD82-434	−58.87	−16.65	3640	KULL	Top	4	D	MAT/GAM-SST/SI	1
MD82-443	−58.78	−15.43	5650	KULL	Top	4	D	MAT/GAM-SST/SI	1
MD82-445	−58.3	−16.03	5750	KULL	Top	4	D	MAT/GAM-SST/SI	1
MD84-521	−50.14	6.79	4150	KULL	Top	4	D	MAT/GAM-SST/SI	1
MD84-529	−48.9	61.99	2600	KULL	Top	4	D	MAT/GAM-SST/SI	1
MD84-530	−66.11	73.98	2412	KULL	Top	4	D	MAT/GAM-SST/SI	1
MD84-531	−66.96	75.41	365	KULL	Top	4	D	MAT/GAM-SST/SI	1
MD84-532	−66.12	76.76	2700	KULL	Top	4	D	MAT/GAM-SST/SI	1
MD84-533	−65.13	78.35	3363	KULL	Top	4	D	MAT/GAM-SST/SI	1
MD84-540	−60.74	86.39	3964	KULL	Top	4	D	MAT/GAM-SST/SI	1
MD84-552	−54.92	73.83	1780	KULL	Top	4	D	MAT/GAM-SST/SI	1
MD84-557	−53.33	75.8	1080	KULL	Top	4	D	MAT/GAM-SST/SI	1
MD84-561	−53.09	71.61	1754	KULL	Top	4	D	MAT/GAM-SST/SI	1
MD84-562	−51.92	68.23	3553	KULL	Top	4	D	MAT/GAM-SST/SI	1
MD84-563	−50.71	68.15	1720	KULL	Top	4	D	MAT/GAM-SST/SI	1
MD84-569	−47.64	73.38	1720	KULL	Top	4	D	MAT/GAM-SST/SI	1
MDBX94-01	−42.5	79.42	2895	BC	Top	4	D	MAT/GAM-SST/SI	1
MDBX94-02	−45.58	86.52	3205	BC	Top	4	D	MAT/GAM-SST/SI	1
MDBX94-03	−46.47	88.05	3559	BC	Top	4	D	MAT/GAM-SST/SI	1
MDBX94-04	−50.37	90.27	3460	BC	Top	4	D	MAT/GAM-SST/SI	1
MDBX94-05	−48.8	89.53	4036	BC	Top	4	D	MAT/GAM-SST/SI	1
MDBX94-06	−44.65	90.69	3709	BC	Top	4	D	MAT/GAM-SST/SI	1
P1010	−77.33	−35	476	KULL	Top	4	D	MAT/GAM-SST/SI	1
PCDF82-1	−63.95	−56.36	430	KULL	Top	4	D	MAT/GAM-SST/SI	1
PCDF82-102	−64.31	−61.88	540	KULL	Top	4	D	MAT/GAM-SST/SI	1
PCDF82-167	−63.93	−56.61	448	KULL	Top	4	D	MAT/GAM-SST/SI	1
PCDF82-174	−64.17	−56.81	288	KULL	Top	4	D	MAT/GAM-SST/SI	1
PCDF82-197	−63.72	−57.23	750	KULL	Top	4	D	MAT/GAM-SST/SI	1
PCDF82-20	−64.23	−55.9	381	KULL	Top	4	D	MAT/GAM-SST/SI	1
PCDF82-34	−62.3	−57.62	1979	KULL	Top	4	D	MAT/GAM-SST/SI	1
PCDF82-35	−62.36	−57.37	1484	KULL	Top	4	D	MAT/GAM-SST/SI	1
PCDF82-47	−62.92	−58.4	723	KULL	Top	4	D	MAT/GAM-SST/SI	1
PCDF82-51	−63.72	−60.05	560	KULL	Top	4	D	MAT/GAM-SST/SI	1
PCDF82-60	−63.39	−59.57	673	KULL	Top	4	D	MAT/GAM-SST/SI	1
PCDF82-61	−63.28	−59.34	728	KULL	Top	4	D	MAT/GAM-SST/SI	1
PCDF82-69	−63	−59.63	916	KULL	Top	4	D	MAT/GAM-SST/SI	1

Table 1 (*continued*)

Core	Longitude	Latitude	Water depth (m)	Coring device	Sampling level	Strat. quality	Fossil group	Use	Ref.
PCDF82-71	−62.64	−59.54	1350	KULL	Top	4	D	MAT/GAM-SST/SI	1
PCDF82-93	−64.07	−61.33	690	KULL	Top	4	D	MAT/GAM-SST/SI	1
PS1195-2	−76.85	−50.49	257	BC	0–1	4	D	IKM-SST	2
PS1200-4	−76.53	−52.72	374	BC	0–1	4	D	IKM-SST	2
PS1208-1	−75.34	−58.79	628	BC	0–1	4	D	IKM-SST	2
PS1209-1	−75.54	−57.72	516	BC	0–1	4	D	IKM-SST	2
PS1214-1	−77.1	−48.61	241	BC	0–1	4	D	IKM-SST	2
PS1222-1	−75.86	−34.31	670	BC	0–1	4	D	IKM-SST	2
PS1223-1	−75.98	−33.55	754	BC	0–1	4	D	IKM-SST	2
PS1273-1	−75.16	−27.33	333	BC	0–1	4	D	IKM-SST	2
PS1277-1	−77.51	−43.19	447	BC	0–1	4	D	IKM-SST	2
PS1278-1	−77.54	−42.13	632	BC	0–1	4	D	IKM-SST	2
PS1366-2	−70.44	−8.42	380	BC	0–1	4	D	IKM-SST	2
PS1372-2	−72.21	−16.72	792	BC	0–1	4	D	IKM-SST	2
PS1374-2	−72.22	−16.93	1458	BC	0–1	4	D	IKM-SST	2
PS1380-1	−70.01	−9.97	2072	BC	0–1	4	R	IKM-SST	3
PS1384-1	−70.46	−9.62	704	BC	0–1	4	D	IKM-SST	2
PS1386-1	−68.33	−5.62	4405	BC	0–1	4	R	IKM-SST	3
PS1387-1	−68.73	−5.84	2435	BC	0–1	4	R	IKM-SST	3
PS1388-1	−69.03	−5.89	2521	BC	0–1	4	D	IKM-SST	2
PS1394-1	−70.08	−6.68	1948	BC	0–1	4	R	IKM-SST	3
PS1395-1	−70.22	−6.98	1489	BC	0–1	4	D	IKM-SST	2
PS1399-1	−76.82	−51.02	251	BC	0–1	4	D	IKM-SST	2
PS1400-4	−77.55	−36.4	1064	BC	0–1	4	D	IKM-SST	2
PS1401-2	−77.6	−35.9	691	BC	0–1	4	D	IKM-SST	2
PS1402-2	−77.48	−34.73	320	BC	0–1	4	D	IKM-SST	2
Ps1403-1	−76.89	−33.39	431	BC	0–1	4	D	IKM-SST	2
PS1407-1	−71.24	−13.57	421	BC	0–1	4	D	IKM-SST	2
PS1410-1	−71.19	−13.55	1511	BC	0–1	4	D	IKM-SST	2
PS1419-1	−74.67	−35.08	479	BC	0–1	4	D	IKM-SST	2
PS1424-1	−76.59	−49.78	286	BC	0–1	4	D	IKM-SST	2
PS1425-1	−70.35	−6.76	456	BC	0–1	4	D	IKM-SST	2
PS1427-1	−70.32	−6.84	612	BC	0–1	4	D	IKM-SST	2
PS1428-1	−70.28	−6.9	1165	BC	0–1	4	D	IKM-SST	2
PS1455-4	−65.42	1.83	2730	BC	0–1	4	R	IKM-SST	3
PS1472-4	−76.58	−30.54	258	BC	0–1	4	D	IKM-SST	2
PS1485-1	−72.56	−18.78	2075	BC	0–1	4	D	IKM-SST	2
PS1486-2	−73.4	−23.09	2572	BC	0–1	4	D	IKM-SST	2
PS1649-1	−54.91	3.29	2446	BC	0–1	4	D	IKM-SST	2
PS1651-2	−53.64	3.84	2089	BC	0–1	4	D	IKM-SST	2
PS1652-1	−53.67	5.08	1960	BC	0–1	4	D	IKM-SST	2
PS1654-1	−50.16	5.77	3763	BC	0–1	2	D	IKM-SST	2
PS1751-2	−44.5	10.48	4802	MC	0–0.5	4	D/R	IKM-SST	2,3
PS1752-5	−45.62	9.61	4553	MC	0–0.5	4	D/R	IKM-SST	2,3
PS1755-1	−47.79	7.1	4321	MC	0–0.5	4	D/R	IKM-SST	2,3
PS1759-1	−50.15	5.76	3793	MC	0–0.5	4	D/R	IKM-SST	2,3
PS1764-2	−50.87	5.71	3936	MC	0–0.5	4	D	IKM-SST	2
PS1765-1	−51.83	4.86	3812	MC	0–0.5	4	D/R	IKM-SST	2,3
PS1768-1	−52.59	4.45	3331	MC	0–0.5	1	D/R	IKM-SST	2,3
PS1771-4	−53.76	3.78	1811	MC	0–0.5	4	R	IKM-SST	3
PS1772-6	−55.46	1.17	4140	MC	0–0.5	4	D/R	IKM-SST	2,3
PS1773-2	−56.32	−0.48	3259	MC	0–0.5	4	D/R	IKM-SST	2,3
PS1774-1	−54.65	−2.87	2453	MC	0–0.5	4	D/R	IKM-SST	2,3
PS1775-5	−50.95	−7.5	2523	MC	0–0.5	4	D/R	IKM-SST	2,3
PS1776-6	−49.73	−8.77	3155	MC	0–0.5	4	D/R	IKM-SST	2,3
PS1777-7	−48.23	−11.03	2575	MC	0–0.5	4	D/R	IKM-SST	2,3
PS1778-1	−49.01	−12.7	3384	MC	0–0.5	4	D/R	IKM-SST	2,3
PS1779-3	−50.4	−14.08	3574	MC	0–0.5	4	D/R	IKM-SST	2,3
PS1780-1	−51.68	−15.27	4258	MC	0–0.5	4	R	IKM-SST	3
PS1782-6	−55.19	−18.6	5131	MC	0–0.5	4	D/R	IKM-SST	2,3
PS1783-2	−54.91	−22.72	3390	MC	0–0.5	4	R	IKM-SST	3
PS1786-2	−54.93	−31.74	5771	MC	0–0.5	1	D/R	IKM-SST	2,3
PS1794-2	−73.54	−25.91	3381	MC	0–0.5	4	D	IKM-SST	2

Table 1 (*continued*)

Core	Longitude	Latitude	Water depth (m)	Coring device	Sampling level	Strat. quality	Fossil group	Use	Ref.
PS1805-5	−66.19	35.31	4149	MC	0–0.5	4	R	IKM-SST	3
PS1813-3	−64.96	33.63	2225	MC	0–0.5	4	R	IKM-SST	3
PS1821-5	−67.07	37.48	4028	MC	0–0.5	4	R	IKM-SST	3
PS1823-1	−65.93	30.84	4442	MC	0–0.5	4	R	IKM-SST	3
PS1825-5	−66.33	8.89	4341	BC	0–1	4	R	IKM-SST	3
PS1831-5	−65.74	13.66	2354	BC	0–1	4	R	IKM-SST	3
PS1957-1	−65.67	−37.48	4727	MC	0–0.5	4	R	IKM-SST	3
PS1967-1	−65.96	−30.07	4847	MC	0–0.5	4	R	IKM-SST	3
PS1973-1	−66.89	−25.55	4841	MC	0–0.5	4	R	IKM-SST	3
PS1975-1	−67.51	−22.52	4893	MC	0–0.5	4	R	IKM-SST	3
PS1977-1	−68.28	−19.34	4838	MC	0–0.5	4	R	IKM-SST	3
PS1979-1	−69.37	−16.5	4735	MC	0–0.5	4	R	IKM-SST	3
PS2073-1	−39.59	14.57	4692	MC	0–0.5	4	R	IKM-SST	3
PS2076-1	−41.14	13.48	2086	MC	0–0.5	4	D/R	IKM-SST	2,3
PS2080-1	−41.72	13.05	5078	MC	0–0.5	4	D/R	IKM-SST	2,3
PS2081-1	−42.69	12.19	4794	MC	0–0.5	4	D/R	IKM-SST	2,3
PS2082-3	−43.22	11.76	4661	MC	0–0.5	4	D/R	IKM-SST	2,3
PS2083-2	−46.37	7.04	1955	MC	0–0.5	4	R	IKM-SST	3
PS2084-2	−47.02	7.96	1664	MC	0–0.5	4	R	IKM-SST	3
PS2087-1	−49.13	6.71	3451	MC	0–0.5	4	D/R	IKM-SST	2,3
PS2102-1	−53.08	−5	2388	MC	0–0.5	1	D	IKM-SST	2
PS2103-2	−51.33	−3.32	2947	MC	0–0.5	4	R	IKM-SST	3
PS2104-1	−50.74	−3.21	2592	MC	0–0.5	4	D/R	IKM-SST	2,3
PS2105-2	−48.69	−2.85	3618	MC	0–0.5	4	D/R	IKM-SST	2,3
PS2108-1	−39.84	1.03	4920	MC	0–0.5	4	D	IKM-SST	2
PS2109-3	−35	3.17	5041	MC	0–0.5	4	R	IKM-SST	3
PS2254-1	−43.97	−50.07	5341	MC	0–0.5	4	R	IKM-SST	4
PS2256-4	−44.51	−44.47	5111	MC	0–0.5	4	R	IKM-SST	4
PS2270-5	−50.88	−32.32	4273	MC	0–0.5	4	D	IKM-SST	2
PS2299-1	−57.51	−30.23	3375	MC	0–0.5	4	D	IKM-SST	2
PS2307-1	−59.06	−35.58	2527	MC	0–0.5	4	D	IKM-SST	2
PS2487-2	−35.83	18.11	2942	MC	0–0.5	4	R	IKM-SST	4
PS2488-1	−38.56	15.8	4888	MC	0–0.5	4	R	IKM-SST	4
PS2489-4	−42.89	8.98	3795	MC	0–0.5	4	R	IKM-SST	4
PS2491-4	−44.96	5.97	4323	MC	0–0.5	4	D/R	IKM-SST	2,4
PS2492-1	−43.18	−4.05	4197	MC	0–0.5	4	D/R	IKM-SST	2,4
PS2493-3	−42.89	−6.02	4174	MC	0–0.5	4	D/R	IKM-SST	2,4
PS2494-1	−41.69	−12.34	3324	MC	0–0.5	4	D/R	IKM-SST	2,4
PS2495-1	−41.29	−14.5	3135	MC	0–0.5	2	D/R	IKM-SST	2,4
PS2496-2	−42.99	−14.64	3518	MC	0–0.5	4	D/R	IKM-SST	2,4
PS2498-2	−44.15	−14.23	3782	MC	0–0.5	3	D/R	IKM-SST	2,4
PS2499-1	−46.51	−15.33	3176	MC	0–0.5	3	D	IKM-SST	2
PS2501-4	−49.4	−21.39	4043	MC	0–0.5	4	D	IKM-SST	2
PS2502-1	−50.25	−23.24	4462	MC	0–0.5	4	D	IKM-SST	2
PS2503-1	−50.75	−24.32	4473	MC	0–0.5	4	D	IKM-SST	2
PS2504-1	−50.84	−24.51	4765	MC	0–0.5	4	D	IKM-SST	2
PS2505-1	−51.19	−25.47	1864	MC	0–0.5	4	D	IKM-SST	2
PS2506-1	−51.41	−25.7	2990	MC	0–1	4	D	IKM-SST	2
PS2507-1	−51.37	−26.2	3275	MC	0–1	4	D	IKM-SST	2
PS2508-1	−51.67	−26.53	3394	MC	0–0.5	4	D	IKM-SST	2
PS2509-1	−52.07	−26.89	4454	MC	0–0.5	4	D	IKM-SST	2
PS2511-1	−55.33	−30.4	2888	MC	0–0.5	4	D	IKM-SST	2
PS2512-1	−54.4	−33.63	4803	MC	0–0.5	4	D	IKM-SST	2
PS2557-2	−36.92	21.83	3371	MC	0–0.5	4	R	IKM-SST	4
PS2560-3	−40.54	25.57	2641	MC	0–0.5	4	R	IKM-SST	4
PS2561-1	−41.86	28.55	4471	MC	0–0.5	4	R	IKM-SST	4
PS2562-1	−43.18	31.58	5193	MC	0–0.5	4	R	IKM-SST	4
PS2563-3	−44.55	34.78	3515	MC	0–0.5	4	R	IKM-SST	4
PS2564-2	−46.14	35.9	3035	MC	0–0.5	4	R	IKM-SST	4
PS2566-1	−48.25	37.49	4422	MC	0–0.5	4	D	IKM-SST	2
PS2602-3	−60.38	36.58	5293	MC	0–0.5	4	D	IKM-SST	2
PS2604-4	−57.6	38.59	5083	MC	0–0.5	4	D	IKM-SST	2
PS2605-1	−54.66	39.92	2996	MC	0–0.5	4	D	IKM-SST	2

Table 1 (*continued*)

Core	Longitude	Latitude	Water depth (m)	Coring device	Sampling level	Strat. quality	Fossil group	Use	Ref.
PS2606-1	−53.24	40.87	2552	MC	0–0.5	1	D	IKM-SST	2
PS2607-1	−51.89	41.52	2859	MC	0–0.5	4	D	IKM-SST	2
PS2609-2	−51.5	41.6	3116	MC	0–0.5	4	D	IKM-SST	2
PS2610-1	−50.68	40.12	3579	MC	0–0.5	4	D	IKM-SST	2
PS2611-3	−49.51	38.83	4261	MC	0–0.5‘	4	D	IKM-SST	2
RC11-118	−37.8	71.53	4354	KULL	Top	4	D	MAT/GAM-SST/SI	1
RC11-119	−40.3	74.57	3709	KULL	Top	4	D	MAT/GAM-SST/SI	1
RC11-77	−53.05	−16.45	4098	KULL	Top	4	D	MAT/GAM-SST/SI	1
RC11-79	−49	−4.6	3100	KULL	2-3	5	D	MAT/GAM-SST/SI	1
RC11-80	−46.75	−0.05	3656	KULL	2-3	5	D	MAT/GAM-SST/SI	1
RC11-90	−56.63	25.72	5334	KULL	2-3	5	D	MAT/GAM-SST/SI	1
RC11-91	−56.57	34.18	5150	KULL	3-4	5	D	MAT/GAM-SST/SI	1
RC11-95	−52.8	54.08	3150	KULL	2-3	5	D	MAT/GAM-SST/SI	1
RC11-98	−47.65	61.48	4650	KULL	Top	4	D	MAT/GAM-SST/SI	1
RC12-292	−39.69	−15.47	3541	KULL	Top	4	D	MAT/GAM-SST/SI	1
RC13-263	−53.81	−8.22	3389	KULL	Top	4	D	MAT/GAM-SST/SI	1
RC15-91	−49.92	−15.57	3775	KULL	3-4	5	D	MAT/GAM-SST/SI	1
RC8-40	−43.75	46.08	2250	KULL	Top	4	D	MAT/GAM-SST/SI	1
RC8-46	−55.33	65.47	2761	KULL	Top	4	D	MAT/GAM-SST/SI	1
SO136-111	−56.66	160.23	3910	KULL	Top	2	D	MAT/GAM-SST/SI	1
SO136-BX043	−50.15	174.67	956	BC	Top	4	D	MAT/GAM-SST/SI	1
SO136-BX068	−54.08	168.5	981	BC	Top	4	D	MAT/GAM-SST/SI	1
SO136-BX110	−56.69	160.25	3907	BC	Top	4	D	MAT/GAM-SST/SI	1
SO136-BX116	−55.66	159.42	4462	BC	Top	4	D	MAT/GAM-SST/SI	1
TNO57-13-PC4	−53.2	5.1	2851	KULL	Top	1	D	MAT/GAM-SST/SI	1
V14-53	−56.72	−24.52	7906	KULL	Top	4	D	MAT/GAM-SST/SI	1
V16-60	−49.99	36.76	4575	KULL	Top	4	D	MAT/GAM-SST/SI	1
V29-87	−49.57	30.02	4550	KULL	Top	4	D	MAT/GAM-SST/SI	1

Position is given in decimals. Coring devices include BC = box corer, GRAV = gravity corer, KULL = Kullenberg piston corer, MC = multicorer or minicorer, TRIG = trigger corer. Sampling level in cm below sea floor, Top indicates sampling of topmost sediment sequence. Stratigraphic quality according to MARGO-defined late Holocene chronozone quality level (1–5). Use of reference samples indicates statistical method (IKM, MAT, GAM) and reconstructed parameter sea surface temperature (SST) and sea ice (SI). Source of reference sample, (1) D204/31 reference set of Crosta et al. (2004), emended from Crosta et al. (1998a, b), (2) Zielinski et al., 1998, (3) Abelmann et al. (1999), (4) Cortese and Abelmann (2002).

Table 2
Summary of statistical methods and equations used for generation of SST and sea ice estimates presented in this paper

Fossil group	Method	Data set/equation	Summer SST see (°C)	Sea ice see (month/year)	Sea ice conc. see (%)	Reference
Diatoms	MAT	D204/31	0.85	0.53	4/5	Crosta et al. (2004)
Diatoms	MAT	D201/25	0.97	1.05		Armand et al. (unpublished data)
Diatoms	IKM	D93/29lg/3	0.66	—	—	Zielinski et al. (1998)
Radiolaria	IKM	R53/23/4	1.2	—	—	Abelmann et al. (1999)
Radiolaria	IKM	R73/24lg/4	1.16	—	—	Cortese and Abelmann (2002)

SEE: standard error of estimates of the used diatom and radiolarian reference data sets. SEE of sea ice concentration indicates error of summer (February)/winter (September) estimate. Data set and equation designations indicate fossil group (D = diatoms, R = radiolarians)/number of reference samples/number of taxa or taxa groups/number of IKM factors, lg indicates logarithmic conversion of species abundance data used to compensate the dominance of single taxa.

paleoceanographic equations (for a summary see Table 2) are presented in Zielinski et al. (1998).

The Southern Ocean radiolarian data set, originally presented by Abelmann et al. (1999), was augmented by Cortese and Abelmann (2002) by extension into the southern subtropical area. This increased the sample/taxa number from 53/23 to 73/24 and provides a reference data set covering a SST range from the Antarctic cold to the subtropical warm water regime in the Atlantic sector (Fig. 2, Table 2). In contrast to previous southern latitude radiolarian data sets, used by CLIMAP (1976, 1981), the new sets of data only consider surface-dwelling radiolarian taxa that show a clear relationship to the surface water distribution pattern. This provides unrestricted comparison of radiolarian and diatom-based SST estimates, both reflecting conditions in the euphotic ocean mixed layer.

The MAT of Hutson (1980) compares the floral assemblage from each down-core sample to a sub-set of modern floral core-top analogs. It calculates a dissimilarity coefficient, which measures the difference between the assemblage of the down-core sample and the assemblage of the analog. Calculation of the dissimilarity coefficient is based on the squared chord distance (Prell, 1985). The estimate is then a simple average of the modern values associated with the analogs chosen by the MAT, and is assumed to represent the climate at the core locality where the fossils of the down-core sample were produced. Down-core estimates are generally calculated on five analogs, except when the dissimilarity threshold of 0.25 is crossed. Below three analogs, the MAT program was set not to provide an estimate, and the fossil assemblage is considered to have no modern equivalent.

MAT was used for E-LGM SST and sea ice reconstruction at 62 locations from all sectors of the Southern Ocean based on a comprehensive diatom reference data set, including a total of 204 samples and 31 taxa (D204/31; Tables 1 and 2). The reference sample locations cover the Atlantic, Indian and westernmost Pacific sector of the Southern Ocean (Fig. 2). Although the samples have been recovered using a large variety of coring systems, ranging from MC to piston coring devices (e.g. Kullenberg corer), the majority are within the MARGO quality levels 1–4 (Kucera et al., 2004) ensuring that the surface sample is derived from a sediment interval not older than 4 ka (Table 1). The reference data set D204/31 has been developed by Crosta et al. (2004) from a database including 195 surface samples, originally prepared by Pichon et al. (1992a, b) and later revised by Crosta et al. (1998a, b). The latter revision considered (i) calibration of the diatom taxonomy approach among diatom paleoceanographers involved in the present study at AWI, Bordeaux and Hobard, (ii) the exclusion of artificially dissolved samples, and (iii) the composition of the considered diatom taxa.

The IKM and MAT calculations have been accomplished using the PaleoToolBox software package developed by Sieger et al. (1999).

Only recently Armand et al. (unpublished material) proposed the GAM (Hastie and Tibshirani, 1990) as a new statistical technique for the estimation of past environment, e.g. sea ice concentration. GAM is used to model a non-linear response between the factors derived from a Q-mode factor analysis and their mean response. Backward elimination procedures assist in selecting appropriate factors and quadratic terms for the estimation equations. Predictions are made from the final bootstrapped model at the 95% confidence level. Here we present GAM-derived E-LGM sea ice concentration estimates obtained from two cores located in the eastern Indian sector between Tasmania and Antarctica using a diatom reference data set that includes 201 surface reference samples and 25 taxa (D201/25) presented by Armand et al. (unpublished data). D201/25 has been created based on the data compiled in the D204/31 Crosta data set. In D201/25, species in the genera *Rhizosolenia* and *Thalassionema* have been excluded, considering that the majority of these taxa are not related to the sea ice environment (Moreno-Ruiz and Licea, 1995; Zielinski and Gersonde, 1997; Crosta et al., 1998a; Armand and Zielinski, 2001).

The SSTs of the hydrographic reference data sets used for diatom and radiolarian-based estimations represent values measured at 10 m below sea surface and were retrieved from Olbers et al. (1992) and Conkright et al. (1998), representing data of the World Ocean Atlas (WOA) (Table 1). Extraction of data was partly achieved using the software available on MARGO web site (http://www.pangaea.de/Projects/MARGO). The temperature values are computed as the area-weighted average of the four temperature values surrounding the sample location. Given that the biogenic particle flux to the sea floor in the Southern Ocean is restricted to austral summer, also in areas unaffected by ice cover (Abelmann and Gersonde, 1991; Gersonde and Zielinski, 2000; Fischer et al., 2002), only summer (January–March average) SST have been estimated.

For MAT and GAM derived sea ice reconstruction, a 13.25-years series (1978–1991) of monthly sea ice concentration averages (Schweitzer, 1995) is employed as the data set of sea ice concentrations and annual duration of sea ice at the specified locations for all the core top samples. The monthly averaged sea ice data set contains information derived from the SMMR and SSM/I satellite instruments and allows the user to specify the locations of retrieval. The data for the Antarctic region uses the ‘Total sea ice NASA TEAM algorithm’ to compile the information of the CD data set. Thus, the data set here represents the time-averaged probability of finding sea ice at a given location and its corresponding typical monthly averaged sea ice concentration. Sea ice concentration is the percentage of a given area of ocean that is covered by sea ice; it represents the amount of sea ice versus open water (Zwally et al., 1983). The monthly average of modern sea ice concentration was extracted for every sample location of our modern data sets for February and September, these months being representative of the minimum and maximum seasonal extent within the annual sea ice cycle, respectively (Comiso, 2003). Sea ice duration in number of months per year at the core locations was calculated from the sea ice concentration data. For MAT-derived sea ice estimates based on the D204/31 data set of Crosta, a sea ice concentration > 40% was selected as a threshold to determine the presence or absence of sea ice during a month. Sea ice concentrations within the 40–50% isopleths correlate well with the compact ice edge location (Gloersen et al., 1992). For each month, the presence (noted 1) or absence (noted 0) was determined based on the concentration threshold, and the yearly sea ice duration was calculated by summing the monthly presence. When monthly sea ice concentration was between 30% and 40%, a 0.5-month duration is reported.

Under the GAM technique (Armand et al., unpublished material), the 15% sea ice concentration threshold was chosen to determine the presence or absence of monthly sea ice cover with respect to the limit of the unconsolidated outer sea ice edge as employed by the sea ice community (Gloersen et al., 1992).

We also include estimates of sea ice extent derived from the abundance pattern of sea ice indicator diatoms (SI-Ind.), as presented by Gersonde et al. (2003a) for the Atlantic sector of the Southern Ocean. The method, proposed by Gersonde and Zielinski (2000), has been developed from combined sediment trap, surface sediment and down-core studies in the Atlantic sector. It considers the relative abundance of the diatom species *Fragilariopsis curta* and *F. cylindrus* (combined into the *F. curta/cylindrus* group) higher than 3% of the total assemblage to represent a qualitative threshold between the average presence of winter (September) sea ice and year-round open waters documented from a 9 years sea ice observation time series (Naval Oceanography Command Detachment, 1985). The average WSI edge corresponds with a mean sea ice concentration of 50–80%. Sea ice indicator values between 3% and 1% of the total diatom assemblage are considered to monitor the maximum winter (September) sea ice extension (mean concentration $<20\%$). The proximity of the summer sea ice limit was deduced through the enhanced presence of *Fragilariopsis obliquecostata*, a taxon restricted to very cold waters ($<-1\,^{\circ}$C) (Zielinski and Gersonde, 1997). *F. obliquecostata* is relatively thickly silicified and thus insignificantly affected by opal dissolution. It thus remains a valuable tracer of sea ice cover even in conditions of low sedimentation and enhanced opal dissolution that are typical in areas close to the perennial ice edge (Gersonde and Zielinski, 2000).

Only recently, Curran et al. (2003) concluded that the Antarctic sea ice cover decreased by about 20% after 1950. This was based on a study of the methanesulfonic acid (MSA) records obtained from a coastal Antarctic ice core (Law Dome). Such findings would also imply the warming of the sea surface, therefore challenging the use of hydrographic and sea ice reference data sets for paleoenvironmental reconstruction, which rely on observations obtained during the past 25 years. In spite of this, the conclusions of Curran et al. (2003) require further support from other Antarctic ice core records, since the use of MSA as an indicator of sea ice extent has been questioned by other authors (Wolff, 2003). Future paleoceanographic reconstruction studies should nonetheless keep in mind a possible mismatch between recent environment information and surface sediment reference data sets that may integrate environmental conditions over a period of more than the past 50 years.

2.3. Quality control of statistically derived estimates

For IKM derived SST estimates based on diatom and radiolarian assemblages, three estimate quality levels (EQL) have been defined using the communality value obtained for the down-core samples. The communality describes the amount of variance accounted for by the factors. Additionally, we considered the observation (Gersonde et al., 2003a) that diatom estimates obtained from Subantarctic and warmer core locations may be biased towards colder temperatures (for further details see Section 3). Consequently, EQLs of diatom estimates obtained from warmer water locations ($>9\,^{\circ}$C modern SSST, $>5\,^{\circ}$C E-LGM SSST), where both diatom and radiolarian estimates are available, have been downgraded to ensure that radiolarian estimates will be used preferentially at these locations. The observation of Gersonde et al. (2003a) indicates that other diatom estimates from Subantarctic and warmer sites that lack radiolarian estimates should also be treated with caution. In case of the occurrence of no-analog samples the EQL has been downgraded to 3 when no-analogs represented the majority of the samples ranging in the E-LGM time slice at the individual core locations.

Estimate quality level 1: communality >0.8. For diatom estimates only: SST difference between radiolarian and diatom based estimate $<1.5\,^{\circ}$C.

Estimate quality level 2: communality 0.7–0.8. For diatom estimates only: SST difference between radiolarian and diatom based estimate $<1.5\,^{\circ}$C.

Estimate quality level 3: communality <0.7. For diatom estimates only: SST difference between radiolarian and diatom based estimate $>1.5\,^{\circ}$C.

For MAT derived estimates of SST and sea ice extent based on the diatom record, three EQLs have been defined taking into account the dissimilarity index. This index indicates the distance between the down-core and the reference surface sediment samples (a zero value indicates down-core and reference samples are identical, whereas a value of 1 indicates total dissimilarity between the down-core and the reference sample).

Estimate quality level 1: dissimilarity <0.1
Estimate quality level 2: dissimilarity 0.1–0.2
Estimate quality level 3: dissimilarity 0.2–0.25
Samples with dissimilarity values above 0.25 indicate no-analog situations and have been discarded.

As the GAM technique employs a Q-mode factor analysis prior to its non-linear GAM regression, we are able to assign EQLs to the determined communalities undertaken in factor analysis as defined above. All determined IKM communalities for the E-LGM data upon which the GAM estimates are based fall into the EQL 1 definition, as they are greater than 0.8 in value (Armand et al., unpublished data).

2.4. Age assignment and stratigraphic quality levels

The establishment of accurate stratigraphic age models for late Pleistocene and Holocene sediments deposited south of the Subantarctic Zone (SAZ) is complicated by the scarcity or lack of biogenic carbonate, especially during glacial intervals, and hence by the lack of continuous benthic and planktic foraminiferal stable isotope records that can be correlated with the standard isotope stratigraphic records. In addition, the lack of sufficient foraminifers makes it difficult to obtain AMS ^{14}C datable samples from foraminiferal shell materials. As a consequence, most of the surface reference samples fall into the MARGO-defined Late Holocene Chronozone Quality Level (CQL) 4 (Table 1) (for definition of quality levels see Kucera et al., 2004). Of those, most have been taken with MC and box corer (BC) devices from areas not affected by winnowing or slumping, and thus represent undisturbed surface sediments. Only few samples from the D204/33 reference set prepared by Crosta have been taken up to a few centimeters below the sea floor surface. Such samples were placed in the Late Holocene CQL 5 (Table 1). However, the statistical treatment of all samples shows that the assemblages considered as reference of modern conditions are clearly related with the modern SST and sea ice distribution (see Crosta et al., 1998a, b; Zielinski et al., 1998; Abelmann et al., 1999; Cortese and Abelmann, 2002).

To identify the EPILOG time-slices as accurately as possible considerable effort has been made to calibrate the abundance fluctuations of siliceous microfossils, such as the radiolarian *C. davisiana* and the diatom *Eucampia antarctica*, with benthic and planktic oxygen isotope records and AMS ^{14}C measurements of organic carbon extracted from planktic foraminifers, or from the humic acid fraction in diatomaceous ooze samples that did not allow for extraction of sufficient amounts of foraminiferal carbonate (Gersonde et al., 2003a). Comparison of AMS ^{14}C dates obtained from organic carbon extracted from planktic foraminifers and the humic acid fraction of the bulk sediment (Bianchi and Gersonde, unpublished data) demonstrates the applicability of the humic acid fraction for ^{14}C dating of diatomaceous ooze from latest Pleistocene and Holocene sediment cores recovered in the Southern Ocean. This places all E-LGM values from PS cores presented by Gersonde et al. (2003a) in the MARGO-defined LGM Chronozone Level 3 or better (Tables 3 and 4; Fig. 3A). Ample stratigraphic accuracy has also been obtained for a number of R.V. *Marion Dufresne* (MD), R.V. *Robert Conrad* (RC) and R.V. *Sonne* (SO) cores, based on AMS ^{14}C measurements and oxygen isotope records. All E-LGM values that have been obtained from a single sample taken at the core depth level defined to represent the LGM by CLIMAP (1976, 1981) have been downgraded to the LGM Chronozone Level 4. The CLIMAP (1976, 1981) age assignment of these cores has mainly been based on the abundance pattern of *C. davisiana*. In contrast, we only took into account such samples in the range of the *C. davisiana* abundance pattern that are assigned to the E-LGM based on AMS ^{14}C dating and isotope records. Lack of attention towards the single sample-based values would not permit the generation of a circumantarctic E-LGM reconstruction, but would provide a restricted reconstruction centered primarily in the Atlantic sector of the Southern Ocean (Fig. 3B).

2.5. Definition of average quality levels

To provide general quality information on each E-LGM value we combined both the stratigraphic and the estimate quality value. This resulted in the definition of two average quality levels (AQL). AQL 1 includes E-LGM values with an E-LGM CQL and an EQLs 1 or 2. All other combinations are in AQL 2 (Tables 3 and 4, Fig. 3C).

3. Results

Southern Ocean summer SST and WSI distribution at the E-LGM have been reconstructed at a total of 107 core locations (Fig. 2). This includes diatom-based reconstructions from 104 locations (Table 3) and radiolarian-based reconstructions from 19 locations (Table 4). Highest spatial coverage of investigated core locations has been obtained in the Atlantic—western Indian sector between 30°W and 45°E, and in the eastern Indian sector between 90 and 150 °E. In the Pacific sector the coverage is poor, except in a narrow segment around 110 °W. Most of the investigated E-LGM sections are from cores recovered between the WSI edge and the Subtropical Front. Only a few cores, located in the western Atlantic and in the eastern Indian sectors, have been collected from the seasonal sea ice covered zone of the Southern Ocean. The reasons for the small number of cores from this zone that could be considered for E-LGM reconstruction are (i) the widespread lack of well-preserved siliceous microfossil assemblages documenting LGM conditions in the present sea ice covered areas, and (ii) strongly reduced glacial sedimentation rates, which preclude accurate definition of the E-LGM level. In glacial sediment sequences deposited close to, or north of the modern Subtropical Front diatom assemblages are affected by

Table 3
Summary of averaged southern summer SST (SSST) and sea ice (SI) estimates from the Epilog Last Glacial Maximum (E-LGM) time slice derived from diatom assemblage information

Core	Lat.	Long.	Depth (m)	Modern SSST (°C)	E-LGM SSST (°C)	Delta LGM/mod. SSST (°C)	Mod. SI presence (m/yr)	E-LGM SI presence (m/yr)	Delta LGM/ modern SI (m/yr)	Modern Feb. SI conc. (%)	E-LGM SI Feb. SI conc. (%)	Delta LGM/ modern Feb. SI conc. (%)	Modern Sept. SI conc. (%)	E-LGM Sept. SI conc. (%)	Delta LGM/ mod. Sept. SI conc. (%)	E-LGM SI Ind. F.c. + F.c. (%)	E-LGM SI Ind. F.o. (%)	E-LGM SI presence	Estimation method	E-LGM CQL	EQL	AQL	Ref.
ELT11-1	−56.05	−115.07	3477	5.55	5.7	0.1	0	0.0	0.0	0	0	0	0	2.8	2.8	0	0	0	MAT	4	1	2	1
ELT11-12	−57.02	−160.10	4721	5.56	3.4	−2.2	0	0.0	0.0	0	0	0	0	0.2	0.2	0.3	0.3	0	MAT	4	1	2	1
ELT11-2	−56.90	−115.25	3111	4.99	5.5	0.6	0	0.0	0.0	0	0	0	0	2.6	2.6	0	0	0	MAT	4	1	2	1
ELT14-6	−59.02	−99.77	4520	5.44	3.4	−2.0	0	1.0	1.0	0	0	0	0	22.4	22.4	0	0	1	MAT	4	1	2	1
ELT15-4	−58.68	−108.80	4914	4.87	4.7	−0.1	0	0.0	0.0	0	0	0	0	2.6	2.6	0	0	0	MAT	4	1	2	1
ELT19-7	−62.17	−109.12	2762	3.01	1.6	−1.4	0	1.9	1.9	0	0	0	0	34	34	0	0	1	MAT	2	1	1	1
ELT20-10	−60.20	−127.05	2445	3.68	2.7	−1.0	0	0.0	0.0	0	0	0	0	7	7	0.9	0	0	MAT	4	1	2	1
ELT21-20	−59.97	−101.32	4703	4.62	4.1	−0.5	0	0.4	0.4	0	0	0	0	9.2	9.2	0	0	0	MAT	4	1	2	1
ELT39-13	−48.02	126.08	4538	10.55	5.0	−5.6	0	0.0	0.0	0	0	0	0	0	0	0	0	0	MAT	4	1	2	1
ELT39-18	−48.87	126.02	4615	9.9	4.3	−5.6	0	0.0	0.0	0	0	0	0	0	0	0	0	0	MAT	4	1	2	1
ELT39-21	−44.89	106.52	4078	10.38	3.5	−6.8	0	0.0	0.0	0	0	0	0	0	0	0.3	0	0	MAT	4	1	2	1
ELT45-35	−53.43	114.25	3920	5.03	1.5	−3.5	0	2.0	2.0	0	0	0	0	37.2	37.2	0	0	1	MAT	4	1	2	1
ELT45-63	−57.80	−115.20	3920	4.47	2.9	−1.6	0	1.1	1.1	0	0	0	0	22.8	22.8	0.3	0	1	MAT	4	1	2	1
ELT45-64	−48.85	114.61	3825	7.55	1.7	−5.9	0	0.9	0.9	0	0	0	0	22.6	22.6	0.3	0.3	1	MAT	4	1	2	1
ELT45-69	−48.03	114.48	3413	10.59	3.0	−7.6	0	1.0	1.0	0	0	0	0	22.6	22.6	0	0	1	MAT	4	1	2	1
ELT45-71	−47.55	114.43	3660	8.5	2.6	−5.9	0	0.7	0.7	0	0	0	0	13.6	13.6	0	0	1	MAT	4	1	2	1
ELT45-74	−45.05	114.37	3806	8.13	7.8	−0.4	0	0.0	0.0	0	0	0	0	0	0	0	0	0	MAT	4	1	2	1
ELT48-27	−38.55	79.91	3277	17.06	16.3	−0.8	0	0.0	0.0	0	0	0	0	0	0	0	0	0	MAT	4	3	2	1
ELT49-29	−47.77	100.03	4237	7.24	2.6	−4.6	0	1.6	1.6	0	0	0	0	25.2	25.2	0	0	1	MAT	4	1	2	1
ELT49-33	−52.48	114.08	4040	5.37	3.2	−2.2	0	0.4	0.4	0	0	0	0	9.2	9.2	0.3	0.3	0	MAT	4	1	2	1
ELT49-6	−53.03	110.05	3326	4.45	1.6	−2.8	0	1.7	1.7	0	0	0	0	33.4	33.4	0.3	0	1	MAT	4	1	2	1
ELT49-7	−55.07	110.02	3592	3.89	1.4	−2.5	0	2.7	2.7	0	0	0	0	45.2	45.2	0.3	0.3	1	MAT	4	1	2	1
ELT50-11	−55.94	104.94	3923	3.31	1.7	−1.7	0	1.8	1.8	0	0	0	0	34.6	34.6	0.3	0.3	1	MAT	4	1	2	1
ELT50-17	−43.88	90.10	4081	10.82	3.9	−7.0	0	0.0	0.0	0	0	0	0	0	0	0	0	0	MAT	4	1	2	1
IO1277-10	−52.02	20.47	2740	2.19	1.4	−0.8	0	3.0	3.0	0	0	0	0	37.6	37.6	1.8	1.2	1	MAT	3	2	2	1
IO1578-4	−59.23	−19.72	4217	0.58	0.5	−0.1	3.5	4.8	1.3	0	0	0	56	62.33	6.33	0.8	0.4	1	MAT	4	3	2	1
KR88-22	−64.67	119.50	3140	0.59	0.4	−0.2	6	7.0	1.0	0	1	1	73	81.4	8.4	8.2	1.3	1	MAT	3	1	2	1
KR88-27	−63.65	101.15	1210	0.03	0.4	0.4	8	7.0	−1.0	0	1	1	88	81.4	-6.6	9.3	2.2	1	MAT	3	1	2	1
KR88-29	−62.50	95.88	3790	0.86	0.4	−0.5	6	6.7	0.7	0	0.4	0.4	81	76.8	-4.2	3.4	1.9	1	MAT	3	1	2	1
MD82-424	−53.05	−16.45	2350	2.46	0.6	−1.8	0	5.4	5.4	0	0.4	0.4	0	61.6	61.6	3.9	5.2	1	MAT	2	2	1	1
MD82-434	−58.87	−16.65	3640	0.61	0.7	0.1	4.5	4.8	0.3	0	0.8	0.8	57	62.2	5.2	1.3	0	1	MAT	3	2	2	1
MD84-527	−44.99	53.28	3262	8.97	8.2	−0.8	0	0.0	0.0	0	0	0	0	0	0	0	0	0	MAT	1	1	1	1
MD84-529	−46.02	96.47	2600	8.63	3.0	−5.7	0	0.0	0.0	0	0	0	0	2.6	2.6	0	0	0	MAT	4	1	2	1
MD84-551	−54.08	−0.35	1504	1.44	0.9	−0.5	0	4.3	4.3	0	0.4	0.4	0	49.6	49.6	1	2.2	1	MAT	1	1	1	1
MD84-552	−56.38	145.30	1780	3.75	1.1	−2.6	0	1.9	1.9	0	0	0	0	34.8	34.8	0	0.9	1	MAT	1	1	1	1
MD88-773	−50.02	104.90	2460	5.55	2.3	−3.3	0	1.4	1.4	0	0	0	0	23.7	23.7	0.6	0	1	MAT	3	1	2	1
MD88-784	−54.19	144.79	2800	5.6	3.5*	−2.1	0	1.8*/1.2**	1.8/1.2	0	0.1**	0.1	0	13.4**	13.4	2.2	0	1	MAT*/GAM**	2	1	1	2
MD88-787	−56.38	145.29	3020	4.26	2.02*	−2.2	0	1.7*/4.3**	1.7/4.3	0	0.2**	0.2	0	19**	19	2.5	0	1	MAT*/GAM**	2	1	1	2
PS1433-1	−47.54	15.36	4810	6.18	2.7	−3.5	0			0			0			1.23	0	1	IKM/SI-Ind.	2	2	1	3
PS1444-1	−55.37	9.98	4862	0.51	0.1	−0.4										4.11	0.69	1	IKM/SI-Ind.	2	1	1	3
PS1649-2	−54.91	3.31	2427	−0.04	−0.1	−0.1	1			0			22			7.68	1.29	1	IKM/SI-Ind.	2	3	2	3
PS1651-1	−53.63	3.86	2075	0.44	0.0	−0.4	0			0			3			8.4	2.4	1	IKM/SI-Ind.	2	2	1	3
PS1652-2	−53.66	5.10	1963	0.24	−0.5	−0.8	0			0			3			18.29	1.1	1	IKM/SI-Ind.	2	2	1	3
PS1654-2	−50.16	5.72	3744	4.56	1.4	−3.1	0			0			0			2.1	0.3	1	IKM/SI-Ind.	1	2	1	3
PS1756-5	−48.90	6.71	3828	5.03	1.6	−3.4	0			0			0			1.84	0.2	1	IKM/SI-Ind.	2	2	1	3
PS1765-3	−51.83	4.81	3760	2.93	0.8	−2.1	0			0			0			4.68	0.42	1	IKM/SI-Ind.	2	2	1	3
PS1768-8	−52.59	4.48	3299	1.47	0.5	−0.9	0			0			0			7.85	0.6	1	IKM/SI-Ind.	1	2	1	3
PS1775-4	−50.95	−7.51	2507	2.03	0.4	−1.7	0			0			0			8.24	0.4	1	IKM/SI-Ind.	2	2	1	3
PS1777-6	−48.23	−11.04	2577	4.92	2.0	−3.0	0			0			0			1.56	0.1	1	IKM/SI-Ind.	2	2	1	3
PS1778-5	−49.01	−12.70	3407	4.81	1.7	−3.1	0			0			0			1.29	0.1	1	IKM/SI-Ind.	2	2	1	3
PS1779-2	−50.40	−14.08	3570	3.97	1.2	−2.7	0			0			0			2.45	0.1	1	IKM/SI-Ind.	2	2	1	3

PS1780-5	−51.70	−15.30	4280	2.86	1.1	−1.7	0			0			0			3.71	0	1	IKM/SI-Ind.	2	2	1	3
PS1782-5	−55.19	−18.61	5160	1.16	1.4	0.2	0			0			0			3.65	0	1	IKM/SI-Ind.	3	2	2	3
PS1783-5	−54.91	−22.71	3394	0.85	0.4	−0.4	0			0			0			6.24	0.4	1	IKM/SI-Ind.	2	2	1	3
PS2082-1	−43.22	11.74	4610	11.35	4.8	−6.6	0			0			0			0.34	0.1	0	IKM/SI-Ind.	2	2	1	3
PS2089-1	−53.19	5.33	2615	1.36	0.2	−1.2										10.18	0.25	1	IKM/SI-Ind.	2	2	1	3
PS2090-1	−53.18	5.13	2819	1.36	0.4	−0.9										5.76	0.8	1	IKM/SI-Ind.	1	2	1	3
PS2102-2	−53.07	−4.99	2390	0.55	0.0	−0.5	0			0			0			12	0.4	1	IKM/SI-Ind.	1	2	1	3
PS2250-5	−45.10	−57.95	3181	12.1	3.0	−9.1										0.22	0	0	IKM/SI-Ind.	2	2	1	3
PS2276-4	−54.64	−23.95	4383	0.89	0.5	−0.4										3.36	0	1	IKM/SI-Ind.	2	2	1	3
PS2278-3	−55.97	−22.22	4418	0.66	0.6	0.0										2.76	0.1	1	IKM/SI-Ind.	2	2	1	3
PS2280-4	−56.84	−22.32	4750	0.22	0.8	0.6										2.65	0.1	1	IKM/SI-Ind.	2	3	2	3
PS2305-6	−58.72	−33.04	3243	1.4	0.2	−1.2										7.9	0.3	1	IKM/SI-Ind.	2	2	1	3
PS2307-1	−59.05	−35.61	2532	0.58	0.0	−0.6										7	0	1	IKM/SI-Ind.	3	2	2	3
PS2319-1	−59.79	−42.68	4323	0.82	0.5	−0.3										10.21	1.4	1	IKM/SI-Ind.	2	2	1	3
PS2491-3	−44.96	5.97	4324	9.32	3.2	−6.1										0.76	0	0	IKM/SI-Ind.	3	3	2	3
PS2492-2	−43.17	−4.06	4207	11.42	4.1	−7.3										0.3	0	0	IKM/SI-Ind.	2	3	2	3
PS2493-1	−42.88	−6.02	4153	11.42	4.0	−7.4										0.41	0	0	IKM/SI-Ind.	2	3	2	3
PS2498-1	−44.15	−14.23	3783	11.11	4.5	−6.6										0.28	0	0	IKM/SI-Ind.	1	3	2	3
PS2499-5	−46.51	−15.33	3175	5.54	2.7	−2.8										0.67	0	0	IKM/SI-Ind.	1	2	1	3
PS2502-2	−50.25	−23.24	4461	4.37	1.2	−3.1										3.16	0	1	IKM/SI-Ind.	2	2	1	3
PS2515-3	−53.55	−45.29	3467	4.35	0.8	−3.5										7.16	0.2	1	IKM/SI-Ind.	2	2	1	3
PS2561-2	−41.86	28.54	4465	16.4	10.9	−5.5										0.84	0	0	IKM/SI-Ind.	3	1	2	3
PS2563-2	−44.56	34.79	3514	9.38	4.1	−5.3										0.28	0	0	IKM/SI-Ind.	3	2	2	3
PS2564-3	−46.14	35.90	3034	9.03	4.3	−4.7										0.33	0	0	IKM/SI-Ind.	3	1	2	3
PS2567-2	−46.94	6.26	4102	6.9	3.9	−3.0										0.48	0	0	IKM/SI-Ind.	2	2	1	3
PS2603-3	−58.99	37.63	5289	1.51	0.9	−0.6										3.66	0.7	1	IKM/SI-Ind.	2	2	1	3
PS2606-6	−53.23	40.80	2545	3.09	0.3	−2.6										3.64	0.5	1	IKM/SI-Ind.	1	3	2	3
PS2608-1	−51.88	41.65	2787	3.09	0.1	−3.0										5	0.8	1	IKM/SI-Ind.	2	3	2	3
PS2610-3	−50.69	40.13	3593	3.74	0.6	−3.1										5.09	0.24	1	IKM/SI-Ind.	2	2	1	3
PS58/271-1	−61.24	−116.05	5214	2.95	1.7	−1.3										1.18	0	1	IKM/SI-Ind.	2	2	1	4
RC8-39	−42.88	42.35	4330	12.1	9.7	−2.5	0	0.0	0.0	0	0	0	0	0	0	0	0	0	MAT	2	2	1	1
RC8-46	−55.33	65.47	2761	3.07	0.9	−2.2	0	2.6	2.6	0	0	0	0	47	47	0	0.6	1	MAT	4	2	2	1
RC9-139	−47.77	123.10	4158	9.91	4.8	−5.2	0	0.0	0.0	0	0	0	0	0	0	0	0	0	MAT	4	1	2	1
RC11-118	−40.30	74.57	4354	15.35	16.3	0.9	0	0.0	0.0	0	0	0	0	0	0	0	0	0	MAT	4	2	2	1
RC11-77	−49.17	−37.42	4098	7.4	0.9	−6.5	0	4.1	4.1	0	0	0	0	52	52	1.3	0.3	1	MAT	4	2	2	1
RC11-91	−56.30	51.97	5373	2.26	1.8	−0.4	0	2.6	2.6	0	0	0	0	45	45	0	0.9	1	MAT	4	2	2	1
RC11-94	−50.47	59.58	4303	4.7	0.8	−4.0	0	3.5	3.5	0	0	0	0	58	58	0	1.3	1	MAT	4	2	2	1
RC11-96	−50.32	61.20	4839	4.65	1.5	−3.2	0	2.7	2.7	0	0	0	0	45.2	45.2	0	0.9	1	MAT	4	1	2	1
RC12-291	−37.27	−10.10	3508	17.9	15.3	−2.6	0	0.0	0.0	0	0	0	0	0	0	0	0	0	MAT	4	3	2	1
RC13-256	−53.88	−4.93	2525	1.61	0.9	−0.7	0	3.8	3.8	0	0.2	0.2	0	44	44	1.9	1.3	1	MAT	4	2	2	1
RC13-259	−56.12	−8.68	2677	1.19	0.8	−0.4	0.5	3.8	3.3	0	0	0	7	48.4	48.4	2.7	1.3	1	MAT	3	1	2	1
RC13-263	−51.99	4.52	3389	2.96	0.8	−2.1	0	4.6	4.6	0	0.2	0.2	0	55.8	55.8	6.8	1.9	1	MAT	3	2	2	1
RC13-269	−52.55	0.22	2591	2.16	1.9	−0.2	0	2.7	2.7	0	0	0	0	36.5	36.5	0.5	2.1	1	MAT	2	2	1	1
RC13-271	−50.72	13.43	3634	3.29	2.3	−1.0	0	0.9	0.9	0	0	0	0	15.8	15.8	0.9	0	1	MAT	2	2	1	1
RC13-275	−47.70	14.70	1984	6.05	3.4	−2.7	0	0.0	0.0	0	0	0	0	2.8	2.8	0.3	0	0	MAT	3	1	2	1
RC14-11	−38.75	59.30	3268	17.79	14.0	−3.8	0	0.0	0.0	0	0	0	0	0	0	0	0	0	MAT	3	2	2	1
RC17-63	−43.47	−57.55	2947	13.6	7.0	−6.6	0	0.0	0.0	0	0	0	0	0	0	0	0	0	MAT	4	2	2	1
SO136-111	−56.67	160.23	3912	5.54	2.2	−3.3	0	1.0	1.0	0	0	0	0	22.3	22.3	0.9	0.4	1	MAT	2	1	1	1
TN057-13-PC4	−53.17	5.12	2848	2.18	1.2	−1.0	0	3.9	3.9	0	0.4	0.4	0	48.2	48.2	2.3	2.1	1	MAT	2	2	1	1
V16-65	−55.68	141.28	1618	4.1	2.0	−2.1	0	1.7	1.7	0	0	0	0	30.6	30.6	0	0	1	MAT	3	1	2	1
V18-110	−43.18	−3.25	2610	11.63	4.4	−7.2	0	0.2	0.2	0	0.2	0.2	0	3.4	3.4	0.3	0	0	MAT	4	2	2	1
V29-86	−49.10	27.38	5614	4.81	4.2	−0.6	0	1.1	1.1	0	0	0	0	20	20	0	0.9	1	MAT	4	2	2	1
V29-87	−45.73	25.65	5314	8.09	3.0	−5.1	0	1.1	1.1	0	0	0	0	20	20	0.3	0	1	MAT	3	1	2	1
V29-89	−43.70	25.73	5945	11.84	6.9	−4.9	0	0.0	0.0	0	0	0	0	0	0	0	0	0	MAT	3	1	2	1

Modern SSST (°C at 10 m water depth) at core location according to Olbers et al. (1992) and Conkright et al. (1998) representing data of the World Ocean Atlas (WOA). Modern sea ice presence (month/year) and sea ice concentration (%) in February and September taken from a 1978–1991 series of monthly sea ice concentration averages (Schweitzer, 1995). E-LGM sea ice indicators (Si-Ind.) are *Fragilariopsis curta* and *F. cylindrus* (F.c. + F.c.) for winter sea ice estimation and the cold-water diatom *Fragilariopsis obliquecostata* (F.o.) for summer sea ice estimation. E-LGM sea ice presence indicates no sea ice (0) and presence of maximum winter sea ice extent (1). Estimation methods are Modern Analog Technique (MAT), General Additive Model (GAM), Imbrie and Kipp Method (IKM) and sea ice distribution estimate based on sea ice indicator diatoms (SI-Ind.). Quality levels include MARGO-defined E-LGM chronozone quality level (E-LGM CQL), estimate quality level (EQL) and average quality level (AQL). References of presented estimates are (1) Crosta data (this paper) using reference data set D204/31, (2) Armand et al. (unpublished data) using D201/25, (3) Gersonde et al. (2003a) and (4) Wittling and Gersonde (unpublished data), both using D93/29lg/3.

*refers to MAT derived estimate.

**refers to GAM derived estimate.

Table 4
Summary of southern summer SST (SSST) estimates derived from radiolarian-based transfer functions from the Epilog Last Glacial Maximum (E-LGM) time slice

Core	Lat.	Long.	Depth (m)	Modern SSST (°C)	E-LGM SSST (°C)	Delta LGM/mod. SSST (°C)	Estimation method	E-LGM CQL	EQL	AQL	Ref.
PS1433-1	−47.54	15.36	4810	6.18	5.2	−1.0	IKM	2	1	1	3
PS1444-1	−55.37	9.98	4862	0.51	1.1	0.6	IKM	2	2	1	3
PS1651-1	−53.63	3.86	2075	0.44	0.5	0.1	IKM	2	2	1	3
PS1756-5	−48.90	6.71	3828	5.03	3.8	−1.2	IKM	2	2	1	3
PS1768-8	−52.59	4.48	3299	1.47	0.9	−0.6	IKM	1	3	2	3
PS1778-5	−49.01	−12.70	3407	4.81	2.0	−2.8	IKM	2	2	1	3
PS1779-2	−50.40	−14.08	3570	3.97	0.8	−3.2	IKM	2	3	2	3
PS1783-5	−54.91	−22.71	3394	0.85	1.0	0.2	IKM	2	2	1	3
PS2082-1	−43.22	11.74	4610	11.35	6.6	−4.8	IKM	2	1	1	3
PS2089-1	−53.19	5.33	2615	1.36	0.5	−0.9	IKM	2	3	2	3
PS2104-2	−50.74	−3.23	2611	3.6	1.9	−1.7	IKM	2	2	1	3
PS2250-5	−45.10	−57.95	3181	12.1	2.4	−9.7	IKM	2	1	1	3
PS2271-5	−51.53	−31.35	3645	3.1	2.7	−0.4	IKM	2	2	1	3
PS2491-3	−44.96	5.97	4324	9.32	5.0	−4.3	IKM	3	2	2	3
PS2492-2	−43.17	−4.06	4207	11.42	6.5	−4.9	IKM	2	1	1	3
PS2493-1	−42.88	−6.02	4153	11.42	6.6	−4.8	IKM	2	2	1	3
PS2498-1	−44.15	−14.23	3783	11.11	6.2	−4.9	IKM	1	1	1	3
PS2567-2	−46.94	6.26	4102	6.9	3.7	−3.2	IKM	2	2	1	3
PS2821-1	−40.94	9.89	4575	15.3	12.1	−3.2	IKM	2	2	1	3

Modern SSST (°C at 10 m water depth) at core location according to Olbers et al. (1992) and Conkright et al. (1998) representing data of the World Ocean Atlas (WOA). Estimation method: Imbrie and Kipp Method (IKM). Quality levels include MARGO-defined E-LGM chronozone quality level (E-LGM CQL), estimate quality level (EQL) and average quality level (AQL). Estimates are from reference (3) Gersonde et al. (2003a).

dissolution. Where this biases the interpretation of the diatom records radiolarian assemblages are able to provide a far more useful paleoceanographic signal. Overall, the set of investigated E-LGM sections/samples is well suited for reconstruction of the glacial northward expansion of the Southern Ocean cold-water realm and WSI field.

Locations with highest E-LGM CQLs are concentrated in the Atlantic and western Indian sectors, while most of the E-LGM estimates in the central and eastern Indian and the Pacific sectors have been placed in the lowest E-LGM CQL (Fig. 3A). Nevertheless, EQLS are remarkably high (EQLs 1 and 2) in most of the investigated E-LGM core sections (Fig. 3B). Thus, the combination of both attribute levels substantiates that high quality information on E-LGM SSST and sea ice conditions are concentrated in the Atlantic sector and western Indian sector of the Southern Ocean (Fig. 3C). This result is due to the low stratigraphic control on many of the samples from the other sectors, mostly representing single samples from an interval defined by CLIMAP (1976, 1981) to represent the LGM.

3.1. E-LGM sea ice reconstruction

E-LGM sea ice reconstruction was based on MAT and GAM-derived estimates of sea ice annual duration (month/year) and concentration during winter (September) and summer (February). In the Atlantic sector this is combined with winter estimates based on the presence of sea ice indicator species (*F. curta* and *F. cylindrus*) presented in Gersonde et al. (2003a). Although MAT and WSI indicator-based reconstructions resulted in a coherent estimation of the WSI extent in the Atlantic sector, there is less conformity between the MAT derived sea ice estimates and the available data on WSI indicators in the Pacific and Indian sectors.

Maximum E-LGM WSI with a concentration > 15% extended in the Atlantic and Indian sector close to 47°S, and in the Pacific sector as far north as 57°S. This extension penetrates into the modern Polar Front Zone (PFZ), between the Polar Front and the Subantarctic Front, and indicates a northward displacement of maximum WSI occurrence by 7–10° in latitude in the different sectors of the Southern Ocean (Fig. 4). WSI with concentrations greater than 40% extended as far north as the present Polar Front area. The available data indicate that the strongest expansion of the ice cover occurs in the Atlantic and western Indian sectors. This indicates that during the E-LGM the WSI field expanded to around $39 \times 10^6\,km^2$, which presents a ca 100% increase compared to modern conditions ($19 \times 10^6\,km^2$; Comiso, 2003).

Only limited information is available on the E-LGM summer sea ice extent. This is due to the fact that in areas covered by perennial ice no microfossil assemblages are

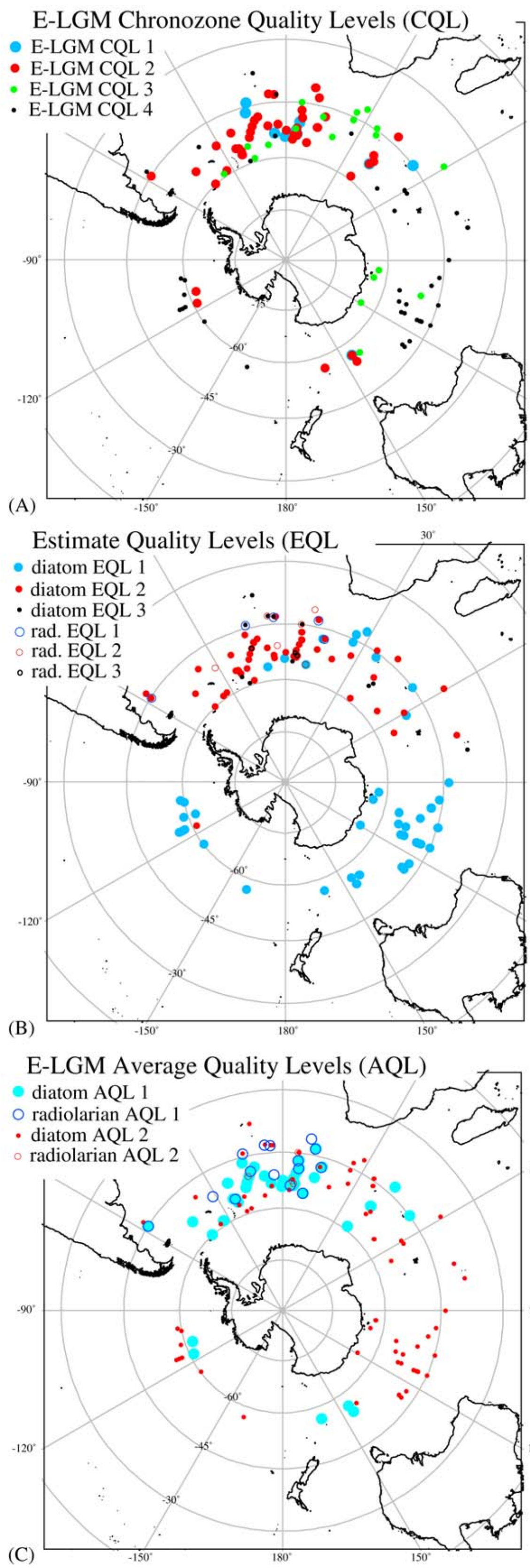

Fig. 3. Spatial distribution of quality level information assigned to E-LGM reconstruction. (A) Distribution of CQL assignments. (B) Distribution of EQL assignments. (C) Distribution of AQL assignments (for details see Tables 3 and 4).

preserved in the sediment record that would allow paleoenvironmental reconstructions, such as SST and sea ice extent. Siliceous microfossil assemblages preserved in the sediment record are generally produced during the austral summer season in open water conditions. The siliceous microorganism flux from the sea ice itself is extremely low or absent, and is generally not discernible in the sediment record (Gersonde and Zielinski, 2000; Fischer et al., 1988, 2002). As a consequence, siliceous microfossil-based estimates of summer sea ice extent only represent a rough approximation of the nearby presence of summer sea ice or the irregular occurrence of summer sea ice. In the few cores recovered from the Atlantic sector, close to the present WSI edge, and three Indian sector cores located in the seasonal sea ice covered zone, we found diatom-derived indications of the sporadic presence of summer sea ice during the E-LGM (Fig. 4). This signal is based on the concomitant occurrence of the cold-water indicator *F. obliquecostata* ($>1\%$ of diatom assemblage) and a MAT estimation that indicates presence of summer (February) sea ice (sea ice concentration $>0\%$)(Table 3).

3.2. E-LGM summer SST reconstruction

Although diatom-based SST estimates have been obtained using different statistical methods and reference data sets in the Atlantic and western Indian sectors, the resulting values show a coherent picture of glacial conditions. This suggests that the different methodical approaches produce sound results when based on a uniform diatom taxonomical approach. Consistency also occurs between the diatom and radiolarian based results from core locations in the modern Antarctic Zone (AZ, south of the Polar Front) and PFZ (between the Polar Front and the Subantarctic Front) (Fig. 5). This supports the reliability of the resulting SST data obtained from both siliceous microfossil groups. However, in cores from the modern SAZ (between the Subantarctic Front and Subtropical Front), the radiolarian-based SST generally give values that are up to 2 °C above the diatom-based estimates (see Tables 3 and 4). The mismatch is interpreted to result in part from a bias of the diatom-based estimates towards colder values due to selective dissolution leading to a relative increase of the coarsely silicified colder-water diatom *F. kerguelensis* (Zielinski and Gersonde, 1997; Crosta et al., 1998a) and also from the shift in phytoplankton communities as a result of nutrient stress and varying physical conditions. Such observations indicate that diatom estimates from Subantarctic and warmer locations should be treated with caution.

The E-LGM summer SSTs obtained at locations in the modern AZ generally display values below 1 °C in the Atlantic sector, and below 2 °C in the Indian and Pacific sectors of the Southern Ocean (Fig. 5), and thus

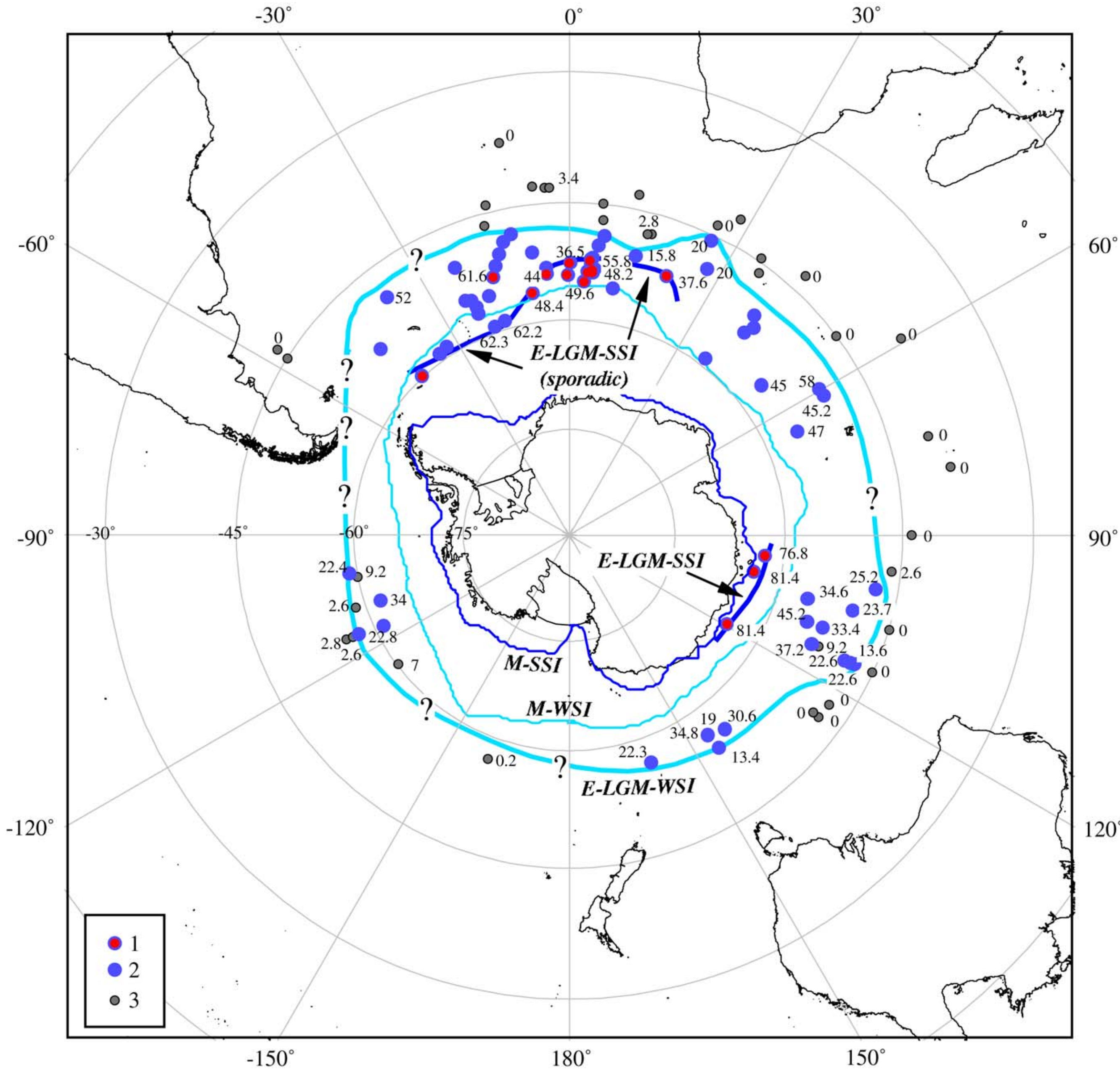

Fig. 4. Sea ice distribution at the E-LGM time slice. E-LGM-WSI indicates maximum extent of WSI (September concentration > 15%). Modern winter sea ice (M-WSI) shows extent of > 15% September sea ice concentration according to Comiso (2003). Values indicate estimated winter (September) sea ice concentration in percent derived with MAT and GAM. Signature legend: (1) concomitant occurrence of cold-water indicator *F. obliquecostata* (> 1% of diatom assemblage) and summer sea ice (February concentration > 0%) interpreted to represent sporadic occurrence of E-LGM summer sea ice; (2) presence of WSI (September concentration > 15%, diatom WSI indicators > 1%); (3) no WSI (September concentration < 15%, diatom WSI indicators < 1%). For data compilation see Table 3.

are up to 3 °C colder than modern SST values (Fig. 6). The cooler SSTs in the Atlantic sector can be related to the Weddell Sea cold-water gyre, which at present extends between the Antarctic Peninsula and around 20°E (western Enderby Basin) to about 60–55 °S (Olbers et al., 1992), and is closely related to the oceanic frontal system named the Scotia Front (Belkin and Gordon, 1996) (Fig. 7A). During the E-LGM, this cold-water gyre expands further to the east by approximately 10° longitude (Figs. 5 and 7A), indicating enhanced formation of cold surface water in the Weddell Sea area. In the modern PFZ, E-LGM summer SSTs range between 1 and 4 °C, and thus were approximately 3–4 °C colder than present. The strongest cooling of summer surface waters during the E-LGM is recorded in sediments collected from the modern SAZ, where the SSTs

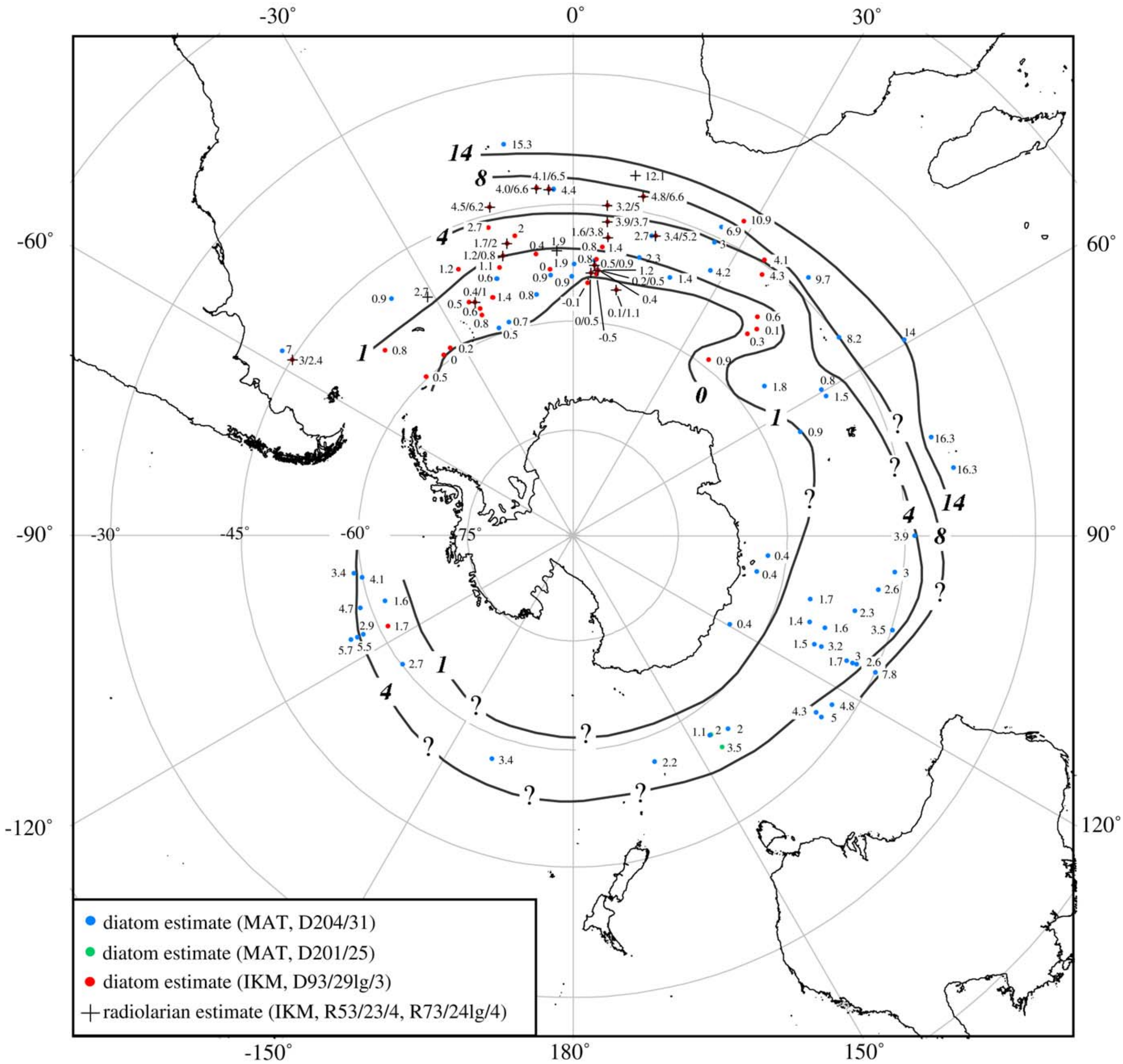

Fig. 5. Estimated austral summer SST (°C) and averaged summer sea surface isotherms (°C) at the E-LGM time slice. Surface isotherms 4 °C, 8 °C and 14 °C stand for average locations of E-LGM PF, Subantarctic Front and Subtropical Front. In the case of multiple SST estimates at any one location, only the highest quality estimate (see Tables 3 and 4) was considered for definition of the isotherm location. At locations with both, diatom and radiolarian estimates, values are labeled diatom SST/radiolarian SST. For data compilation see Tables 3 and 4.

generally decreased by 4–6 °C (Fig. 6). Highest anomalies, reaching values around 7 °C, come from diatom-based estimates in the Atlantic and Indian sector. However, comparison with radiolarian-based values shows that the E-LGM cooling in the modern SAZ did generally not exceed 5 °C and that the diatom-based estimates may be biased towards colder values by selective species dissolution, hence resulting in higher anomalies.

In the Pacific sector, only a few cores document the E-LGM temperature regime in the northern zone of the Southern Ocean. These cores are located around the present Subantarctic Front (Fig. 1). In contrast to the E-LGM anomalies obtained from the Atlantic and Indian sectors, we do not observe significant SST change from these Pacific locations (Fig. 6). The few cores located north of the present Subtropical Front (Fig. 1) indicate only a minor decrease in E-LGM summer SST, which

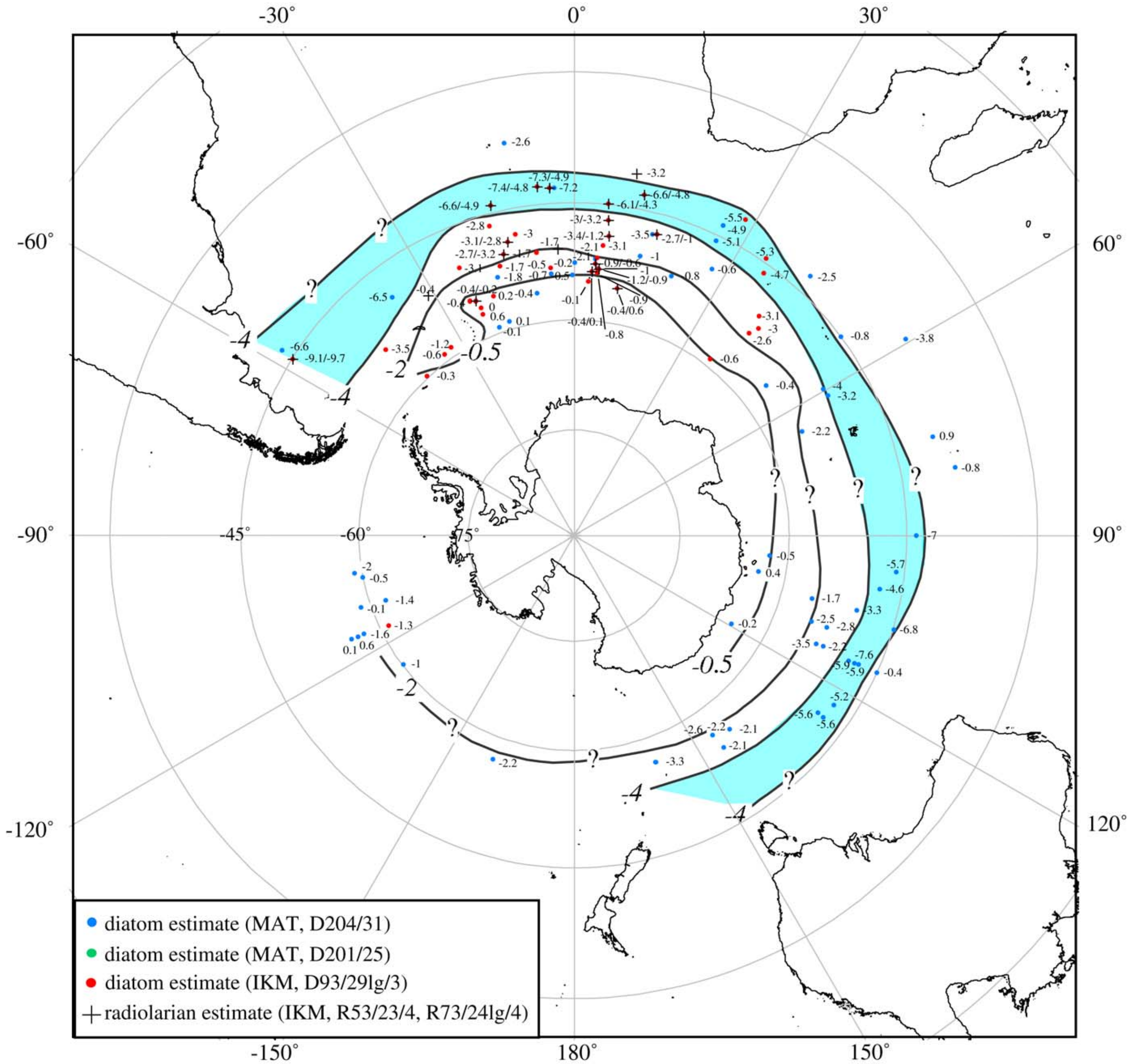

Fig. 6. Austral summer sea surface (°C) anomaly (modern/E-LGM) and averaged anomaly isotherms (°C). Area with anomalies > 4 °C is shaded blue. In cases with more than one SST anomaly available at any one location, only anomalies derived from highest quality estimate (see Tables 3 and 4) was considered for definition of an anomaly isotherm location. At locations with anomalies derived from both, diatom and radiolarian estimates, values are labeled diatom derived anomaly/radiolarian derived anomaly. For data compilation see Tables 3 and 4.

suggests that the present southern subtropical realm was not strongly affected by cooling during the E-LGM.

4. Discussion

Comparison of the E-LGM WSI extent obtained from diatom-based studies with previous estimates relying on the sediment facies distribution (CLIMAP 1976, 1981; Cooke and Hays, 1982) yield a rather consistent pattern of LGM sea ice maximum extent (Fig. 8A). In the Atlantic and Indian sectors the WSI expanded by ca 10° in latitude during the E-LGM. In these sectors the E-LGM sea ice edge approaches the area around 47°S, which is in the modern PFZ, close to the Subantarctic Front. Although the AQL of the sea ice estimates for the Indian sector is generally low, due to low-E-LGM CQLs (Fig. 3A), the obtained reconstruction yields a consistent pattern among all sample locations, supporting the reliability of the reconstruction.

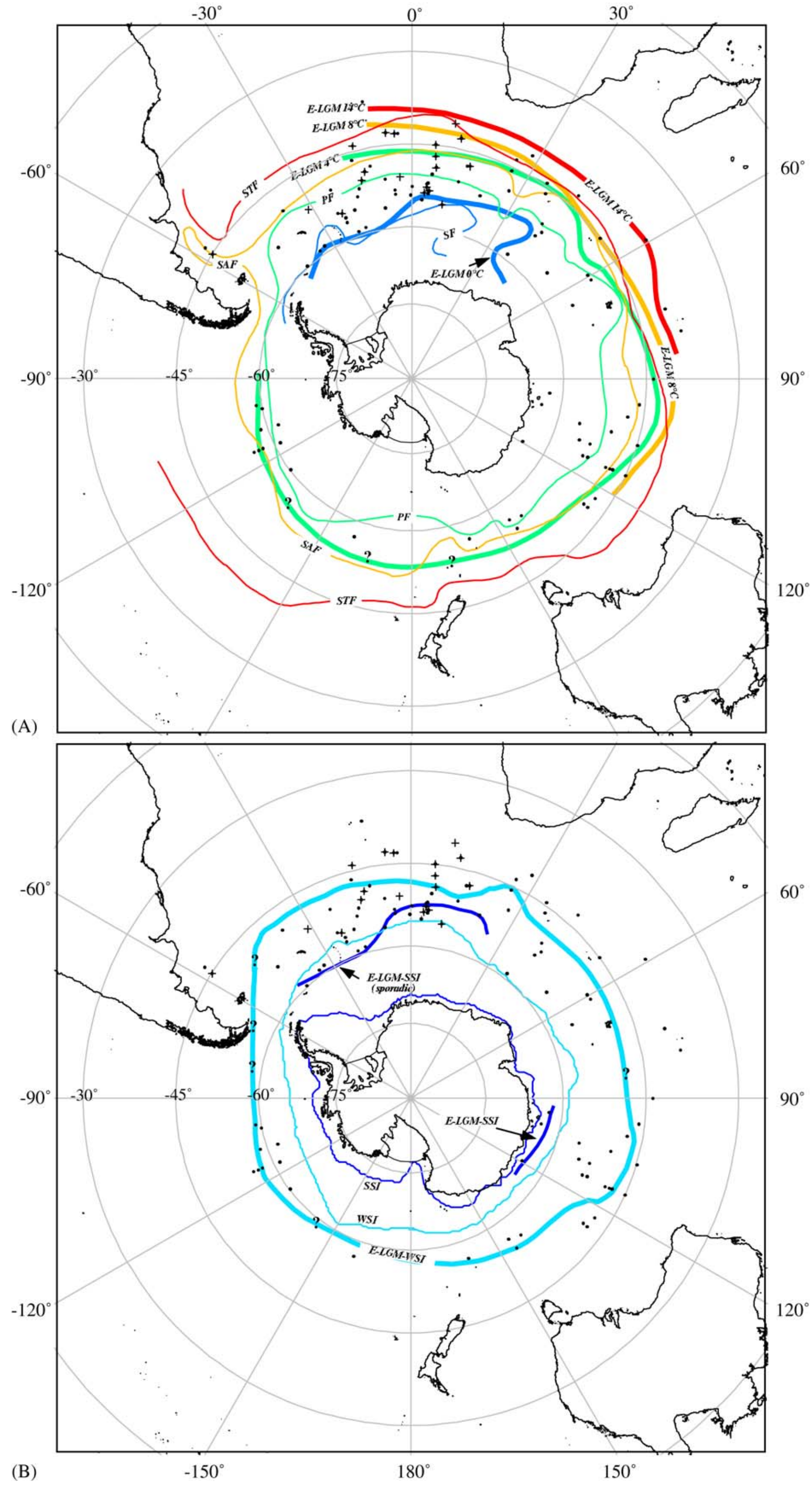

Fig. 7. (A) Comparison of modern oceanic frontal zone locations, SF/Weddell Gyre cold water extent, PF, SAF, STF, according to Belkin and Gordon (1996), with average E-LGM summer sea surface isotherms (0 °C isotherm approximates E-LGM Weddell Gyre cold water extent, 4 °C approximates E-LGM Polar Front, 8 °C approximates E-LGM Subantarctic Front, 14 °C approximates E-LGM Subtropical Front). (B) Comparison of modern ice edge, WSI, summer sea ice (SSI), data from Comiso (2003) (see also Fig. 4 legend), with E-LGM sea ice (E-LGM-WSI, E-LGM-SSI sporadic occurrence of summer sea ice).

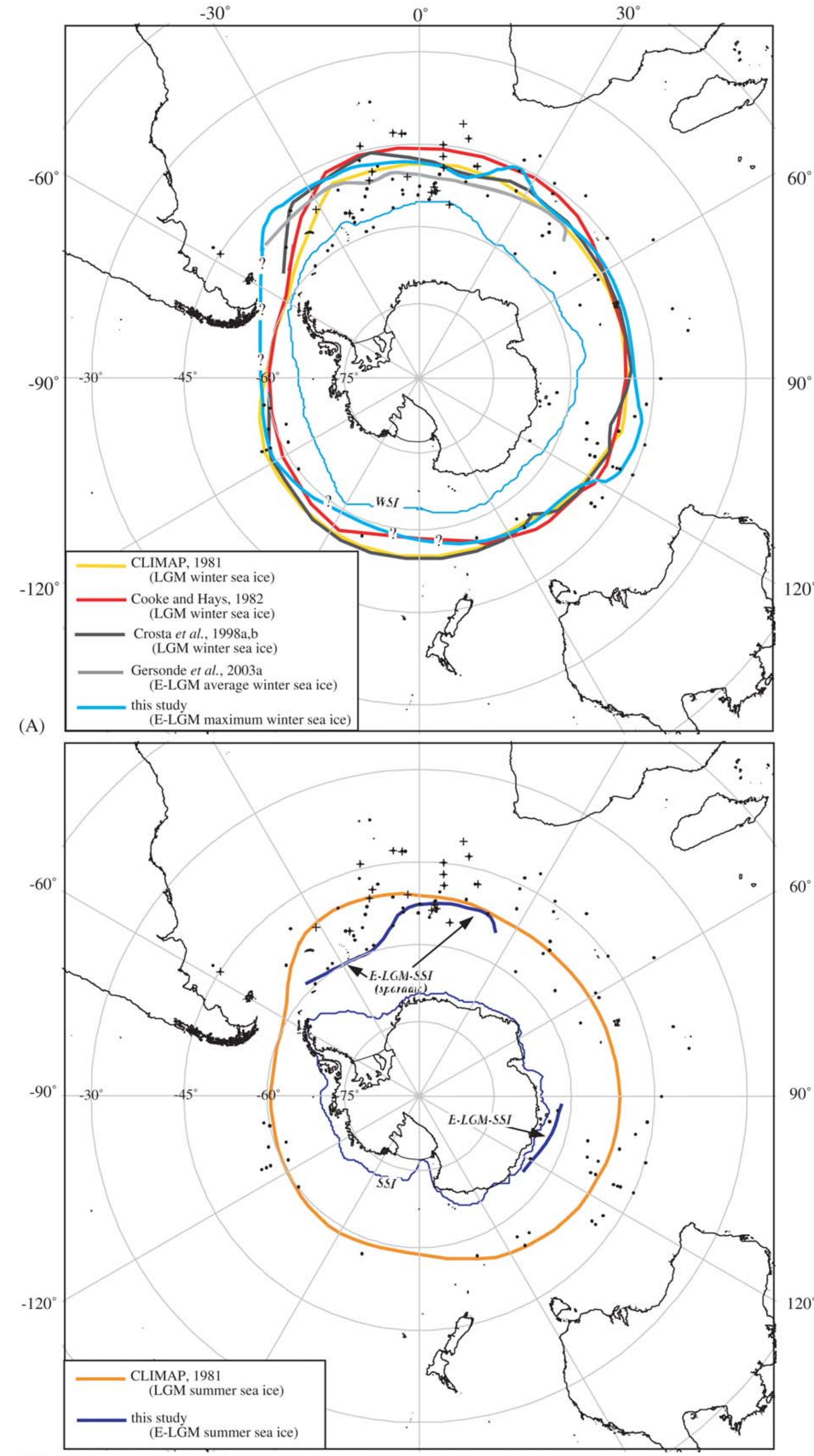

Fig. 8. (A) Comparison of LGM WSI edge reconstructions presented by different studies. (B) Comparison of LGM summer sea ice edge reconstructions from CLIMAP (1981) and this study.

The scarce data from the Pacific sector point to smaller expansions of the E-LGM WSI in this sector. To substantiate the Pacific sector sea ice distribution, more data points are urgently needed. In the Atlantic sector the estimation of the average maximum WSI edge derived from the abundance pattern of the diatom sea ice indicators *F. curta* and *F. cylindrus* matches well the MAT-derived 15% sea ice concentration limit, indicating the edge of dense sea ice cover (Fig. 4). In the Pacific and Indian sectors, there is generally less conformity between the MAT derived sea ice estimates and the available data on sea ice indicators used for WSI reconstruction. The approach to reconstruct past sea ice by means of winter percent concentration recently proposed by Crosta et al. (2004) and Armand et al. (unpublished observations) and using MAT or GAM, respectively, significantly improves our ability of past circum-Antarctic WSI reconstruction.

Major uncertainties concern the reconstruction of summer sea ice extent. Here we interpret the concomitant occurrence of the cold-water indicator *F. obliquecostata* ($>1\%$ of diatom assemblage) and MAT-derived summer sea ice concentration $>0\%$ to indicate the "sporadic occurrence" of summer sea ice. In the eastern Atlantic sector of the Southern Ocean such sporadic summer sea ice occurrences have extended during the E-LGM as far north as 52°S, in close relation with an expanded Weddell Sea cold-water gyre (Figs. 7A and B). Nevertheless, as it has already been outlined by Crosta et al. (1998a, b) and Gersonde et al. (2003a), our results definitely rule out a strongly expanded E-LGM summer sea ice extent as proposed by CLIMAP (1981), reaching 50–52°S in the Atlantic and Indian sectors, and around 60°S in the Pacific sector of the Southern Ocean (Fig. 8B). Perennial LGM sea ice cover as suggested by CLIMAP (1981) would not allow the production and preservation of siliceous microfossil assemblages documented in E-LGM intervals obtained from cores located between 50°S and 64°S. Crosta et al. (1998a, b) speculate that the location of the LGM summer sea ice edge was similar to its modern position in the Indian sector of the Southern Ocean. This is documented in E-LGM intervals obtained from three KR88 cores recovered close to the East Antarctic coast. From the Pacific and Atlantic sector no cores located proximal to the Antarctic continent are available that would provide first-order documentation of the E-LGM summer sea ice extent. Widespread opal dissolution in the Weddell Sea (Schlüter et al., 1998) precludes reconstruction of the sea ice edge and of temperatures based on the siliceous microfossil record in a large area of the southernmost Atlantic sector. However, the obtained summer SST and the indication of a patchy northward expansion of the E-LGM summer sea ice field point to a larger than present summer sea ice extent in the Weddell Sea area at the E-LGM time slice, as already outlined by Gersonde et al. (2003a). The relatively small expansion of the E-LGM summer sea ice extent and a strong expansion of the WSI field resulted in increased seasonality of the E-LGM sea ice compared with present conditions. It can be speculated that the seasonal changes of the sea ice field that at present range between $4\times10^6\,km^2$ (summer) and $19\times10^6\,km^2$ (winter) (Comiso, 2003) changed to a range between ca $5–6\times10^6\,km^2$ (E-LGM summer) and $39\times10^6\,km^2$ (E-LGM winter).

Such enhanced seasonal sea ice production would have a strong impact on the production of Southern Ocean cold deep water via brine rejection and the velocity pattern of the Antarctic Circumpolar Current (ACC). Extremely cold Southern Ocean deep water, close to the freezing point, has been reported from the LGM (Duplessy et al., 2002; Mackensen et al., 2001). Keeling and Stephens (2001) hypothesize that Antarctic sea ice expansion affects not only the amplification of climate variability, but it also steers thermohaline overturning, due to the associated changes in the oceans salinity structure (Shin et al., 2003).

There is evidence that during the E-LGM time slice, which coincides with a maximum sea-level-low stand at ca 135 m below present (Yokoyama et al., 2000), climate conditions of the Southern Ocean were not the coldest of the last glacial. Summer sea ice indicators show distinct northward expansion of the summer sea ice field during the pre-E-LGM period between 30 000 and 25 000 cal yr. B.P., reaching 55°S in the eastern Atlantic sector (Gersonde et al., 2003a). Stronger Southern Ocean cooling during this period is also indicated by SST records from the Atlantic Subantarctic sector (Gersonde et al., 2003b) as well as SST and sea ice records from the eastern Indian sector (Armand and Leventer, 2003; Crosta et al., 2004; Armand et al., unpublished data) (Fig. 9). Such patterns point to significant changes in sea ice seasonality and production during the last glacial in the Southern Ocean. This observation calls for the need of accurate dating of any time-slice assigned to represent the LGM, to prevent data and varying environmental conditions from different periods being averaged into reconstructions of the LGM environment. The recent approach to reconstructing past Antarctic sea ice production based on the flux rates of sea salt recorded in ice cores (Wolff et al., 2003) may represent an additional method for sea ice reconstruction at high-resolution. Distinctly higher glacial sea salt flux rates observed in the Dome C record may be indicative for stronger sea ice seasonality and related sea ice production during glacial periods. However, the record presented by Wolff et al. (2003) does not show significant variability in glacial sea ice seasonality as it can be deduced from the marine record.

Comparison of the E-LGM summer SSTs with those presented by CLIMAP (1981) shows that both reconstructions result in strongest LGM cooling being located

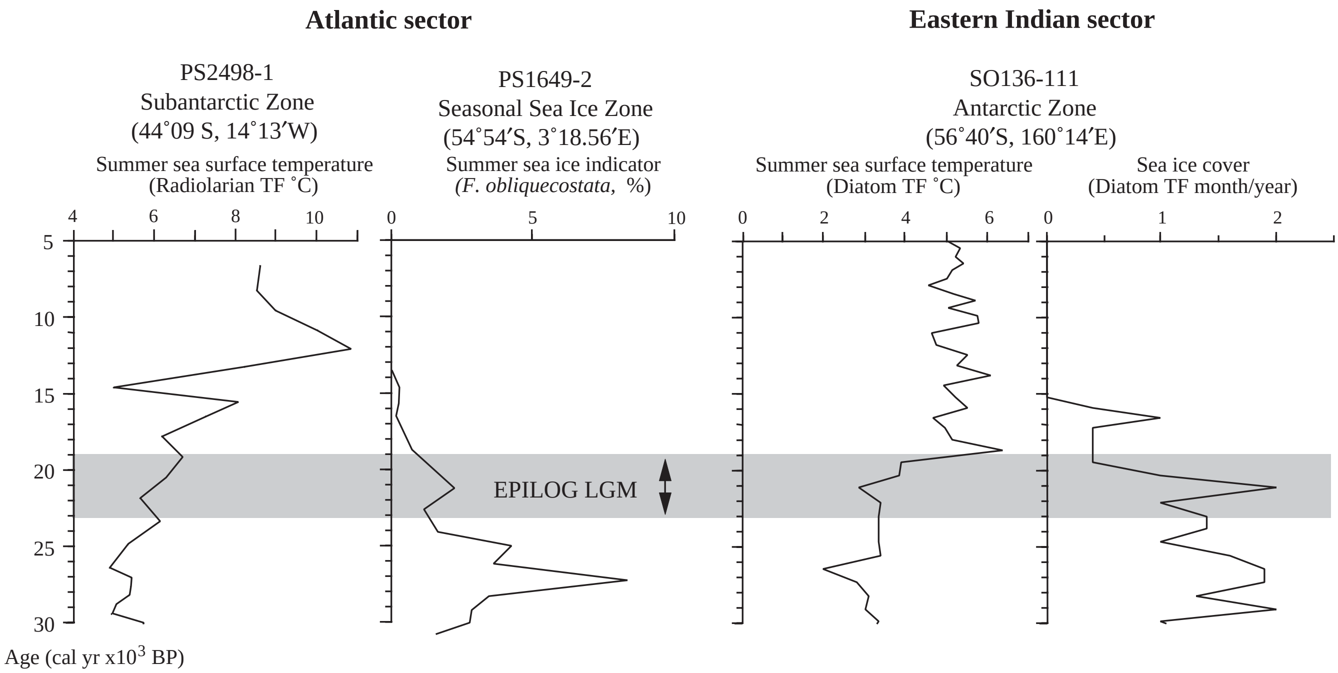

Fig. 9. Siliceous microfossil derived summer sea surface temperature and sea ice estimates for the past 30 000–5000 calendar years (BP), showing pre-EPILOG LGM maximum cooling in different sectors and latitudes of the Southern Ocean. Radiolarian transfer function (TF) derived SST record in Core PS2498-1 from Gersonde et al. (2003b), summer sea ice indicator record in Core PS1649-2 from Gersonde et al. (2003a), diatom SST and sea ice record in Core SO136-111 from Crosta et al. (2004).

in the northern Southern Ocean, with temperature decreases of more than 4 °C. While CLIMAP (1981) presents a more patchy areal distribution of maximum cooling, our compilation of E-LGM summer SSTs indicates a more continuous zone of enhanced cooling, and thus generally colder summer sea-surface conditions than estimated by CLIMAP (1981). We also remark that CLIMAP (1981) placed the belt of strongest cooling around 50°S in the Atlantic and the Indian sector, while our reconstruction points to a more southerly located zone of maximum cooling (Fig. 6). The rather small number of observations available from the Pacific Southern Ocean does not provide an overall picture of the E-LGM surface water temperature pattern from this sector. The few data available point to a reduced E-LGM cooling in the southern Pacific, a pattern also presented by CLIMAP (1981). In the event that additional data from the Pacific sector confirm a non-uniform E-LGM cooling of the Southern Ocean surface waters, major questions on the mechanisms responsible for such differentiation will arise. Possible mechanisms may be related to the configuration of the glacial Ross Ice Shelf that may have a major impact on the generation of last glacial cold surface waters in the Pacific sector of the Southern Ocean.

Reconstruction of summer SST and sea ice clearly demonstrates that there was an expansion of the Southern Ocean cold water realm. Assuming that the modern relationship between summer SST and the location of the oceanic fronts can be applied to the E-LGM, the Polar Front in the Atlantic, Indian and Pacific sectors would have shifted to the North during the E-LGM by around 4°, 5–10°, and 2–3° in latitude, respectively, compared to their present location. In the Atlantic and Indian sector, the Subantarctic Front would have shifted by around 4–5° and 4–10° in latitude, respectively. The Subtropical Front displacement would have been minor, by around 2–3° and 5° in latitude in the Atlantic and Indian sector, indicating a compression of the SAZ during the E-LGM (Fig. 7A). The resolution of our data set makes it impossible to trace the location of past fronts based on the spatial mapping of surface water gradients, and thus we cannot contribute much to the ongoing debate if the oceanographic fronts were displaced during glacial cooling periods along with the surface isotherms. Our microfossil analyses indicate a northward migration of the planktic communities from which we inferred the glacial cooling. Stable isotope measurements ($\delta^{18}O$) on planktic and benthic foraminifers are interpreted to show similar Holocene and glacial oceanic circulation, arguing against frontal migration (Matsumoto et al., 2001). The latter authors attributed such robust ACC circulation pattern to factors such as bottom topography and land–sea configuration, both exerting strong controls over the large-scale ocean circulation. Hydrographic sections and satellite-derived data on frontal patterns, frontal locations and their spatial and temporal variability outline the complexity of these oceanographic features (Belkin and Gordon, 1996; Moore et al., 1999). In areas with distinct bottom topography, the mean path of fronts is closely linked to topographic structures, while over deep ocean basins fronts may meander over a wide latitudinal range extending over 5–7° in latitude (Moore et al., 1999). Comparison of different observations such as compiled by Belkin and Gordon (1996) and Moore et al. (1999) indicate that fronts may jump from one to another topographic structure, over more than 5° in latitude, a mechanism that could also have occurred following climate related changes in Southern Ocean hydrography. Assuming that the location of the E-LGM fronts was not significantly changed compared to present, they were represented by cooler isotherms, and the Polar Front was seasonally south of the sea ice edge.

The location and oceanographic pattern of the ACC zones in the Pacific sector has major implications on the functionality of the Drake Passage ''cold water route'' (CWR; Rintoul, 1991) that regulates Pacific–Atlantic water mass and heat exchange. Together with the Agulhas ''warm water route'' (Gordon, 1986), the CWR represents the most important return-flow portal in global thermohaline circulation, having crucial importance on global climate development (Drijfhout et al., 1996). Gersonde et al. (2003a) speculated that a strong E-LGM cooling in the area east of the southern Argentine coast (Fig. 6) might indicate the reduced import of surface waters with temperature properties of the present PFZ via the CWR. They relate this reduction to a northward displacement of the Southern Ocean zones that caused truncation of the northern warmer waters passing the Drake Passage at present. A resulting deflection of Southern Ocean waters along the South American coast in the southeast Pacific is corroborated by foraminiferal studies in the eastern tropical Pacific showing that the cooling in the LGM Equatorial Pacific was related to an increased northward advection of Southern Ocean waters (Feldberg and Mix, 2002, 2003).

As a consequence of northward expansion of Southern Ocean cold waters and of minor changes of E-LGM summer SST in the present southern subtropical realm observed in the Atlantic (Gersonde et al., 2003a; Niebler et al., 2003) and the Indian sectors, the surface water temperature gradients steepened during the E-LGM around the Subtropical Front and the SAZ compared to modern conditions (Fig. 7A). Such steepening of hydrographic gradients should have had an impact on the velocity of zonal water transport in the northern realm of the E-LGM ACC, as indicated by sedimentological and isotope geochemical studies showing intensified glacial deep water mass transport in the Indian sector and in the western Pacific (Dézileau et al., 2000; Hall et al., 2001). The gradient change should have also affected atmospheric circulation, e.g. a northward-shift of the westerly winds, as proposed by Sigman and Boyle (2000) in a glacial Southern Ocean model. Such northward displacement of the wind field may result in the displacement of the Polar Front, as postulated from a simulation with an simple, one-layer Southern Ocean model forced by westerlies, northward shifted by 5° in latitude and increased in strength (Klinck and Smith, 1993).

The reconstruction of sea ice and summer SST at the E-LGM time slice documents distinct changes in physical parameters that potentially enhance glacial CO_2 draw down in the Southern Ocean. The Southern Ocean cold-water sphere expansion (between 5° and 10° in latitude) and the enlargement of the sea ice field would have increased Southern Ocean carbon uptake capacity (Bakker et al., 1997) and reduced air–sea exchange of CO_2 (Stephens and Keeling, 2000; Morales Maqueda and Rahmstorf, 2002), respectively.

5. Summary and outlook

Based on the quantitative study of diatoms and radiolarians, we estimated summer SST and sea ice distribution at 107 sediment core localities in the Atlantic, Indian and Pacific sector of the Southern Ocean to reconstruct the last glacial environment at the EPILOG (19.5–16.0 ka, equal to 23 000–19 000 cal yr B. P.) time-slice (E-LGM time slice). The applied statistical methods include the Imbrie and Kipp Method, the MAT and the General Additive Model. Age assignment of the samples selected to represent the E-LGM time slice and the obtained estimates have been ranked according to defined quality levels. Highest AQLs concentrate in the Atlantic and western Indian sector. Although the AQL of the estimates is generally low in the other sectors due to low stratigraphic control, the obtained reconstruction yields a rather consistent pattern supporting the reliability of the reconstructions.

Even though diatom-based SST estimates have been derived from different statistical methods and reference data sets, they result in a coherent SST pattern. This is also true for diatom and radiolarian-based SST estimates from the Antarctic and PFZ locations in the Atlantic sector. However, at locations from Subantarctic and warmer areas, diatom-based estimates may be biased towards colder values due to selective species dissolution.

The obtained E-LGM reconstructions can be summarized as follows:

Maximum E-LGM WSI (concentration > 15%) extended in the Atlantic and Indian sector close to 47°S, and in the Pacific sector as far north as 57°S. This reflects an E-LGM northward displacement by 7–10° in latitude in the various Southern Ocean sectors and converts to a ca 100% increase of the sea ice field ($39 \times 10^6\,km^2$) compared with modern conditions.

E-LGM summer sea ice extent information is rather limited. In the Indian sector the extent was close to the modern summer sea ice distribution. In the Atlantic, second-order information points to more expanded than present summer sea ice coverage that is restricted to the Weddell Sea area. There is indication for sporadic summer sea ice occurrence reaching as far north as 52°S in the eastern Atlantic sector. Estimates from the southwest Pacific region clearly indicate that no summer sea ice cover was present in the current PFZ (Armand et al., unpublished data).

The distinct enlargement of the E-LGM WSI field and indications of only minor summer-sea ice expansion in two sectors of the Southern Ocean, lend support to the theory of increased sea ice seasonality compared with present day.

The reconstruction of maximum WSI extent is broadly in accordance with CLIMAP (1981). The data, however, clearly show that CLIMAP (1981) strongly overestimated the glacial summer sea ice extent.

E-LGM Summer SST indicate a northward displacement of the Antarctic cold waters between 5° and 10° in latitude in the Atlantic and Indian sectors. Strongest cooling occurs in the present SAZ, reaching values between 4 and 6 °C. As a result of northward expansion of Antarctic cold waters and a relatively small displacement of the averaged Subtropical Front, thermal gradients were steepened during the last glacial in the northern zone of the Southern Ocean. This may, however, be inapplicable to the Pacific sector. The few data points available indicate reduced cooling the southern Pacific, and give hint to a non-uniform cooling of the glacial Southern Ocean.

Generally, the summer SSTs reveal greater surface-water cooling than those reconstructed by CLIMAP (1981).

Despite the progress in the dating, the use of statistical reconstruction methods and the establishment of surface sediment, hydrographic and sea ice reference data sets, as well as the collection of cores, there are still deficiencies that reduce our ability of accurate LGM reconstruction of the entire Southern Ocean. This includes the lack of appropriate surface sediment sample sets and sediment cores especially in the Pacific sector, but to some extent also in the Indian sector. Some improvement will be available in the near future from the establishment of surface sediment references for the central and eastern Pacific sector (Gersonde et al., unpublished data) (Fig. 2). Improved methods for a more accurate reconstruction of the glacial summer sea ice field are urgently needed. Such methods may be based on a combination of paleo sea ice reconstructions and paleo sea ice modeling, using SST prescription from paleoceanographic reconstructions. This should allow better determination of the distribution of the perennial ice cover as well as the sea ice seasonality, both of which impact sea–air gas exchange, biological productivity, atmospheric circulation and water-mass formation. Considering the strong value of radiolarian assemblages for generation of SST in the northern zone of the Southern Ocean, the number of radiolarian-based LGM reconstructions should be increased considerably together with the enlargement of reference data sets and expansion into the Indian and Pacific sectors. Such studies may also improve our knowledge on the processes related to water mass and heat exchange via the Drake Passage cold-water route. A major effort is also required to better describe past salinity changes at the Southern Oceans surface that are of major importance for the understanding of the Southern Ocean hydrography and its role in past thermohaline circulation changes (Stocker, 2003). A new promising tool to generate estimates of surface water salinity changes is the determination of the isotopic composition of oxygen in marine diatoms, as proposed by Shemesh et al. (1995, 2002). Last, but not least, AMS ^{14}C dating methods need further improvement to obtain more accurate dating of sediments dominated by siliceous microfossils.

Acknowledgment

We thank Nalan Koc and an anonymous reviewer, as well as Giuseppe Cortese for review of the paper and useful comments. Discussions among the MARGO scientific community during two MARGO workshops were also fruitful. Hans-Werner Schenke and Martin Klenke helped with graphic areal estimates. Oscar Romero provided surface sediment samples from the South Atlantic that have been included to the D204/31 data set prepared by Xavier Crosta. The generation of this paper has largely profited from the remarkable effort of the MARGO steering group and editors Michal Kucera, Ralph Schneider, Claire Waelbroeck and Mara Weinelt.

Electronic versions of data shown in this paper are available at http://www.pangaea.de/Projects/MARGO and will be updated according to future progress in the acquisition of E-LGM paleoceanographic data for the Southern Ocean.

References

Abelmann, A., 1988. Freeze-drying simplifies the preparation of microfossils. Micropaleontology 34, 361.

Abelmann, A., Gersonde, R., 1991. Biosiliceous particle flux in the Southern Ocean. Marine Chemistry 35, 503–536.

Abelmann, A., Brathauer, U., Gersonde, R., Sieger, R., Zielinski, U., 1999. A radiolarian-based transfer function for the estimation of summer sea-surface temperatures in the Southern Ocean (Atlantic sector). Paleoceanography 14 (3), 410–421.

Armand, L.K., Leventer, A., 2003. Paleo sea ice distribution—reconstruction and paleoclimatic significance. In: Thomas, D.N., Diekmann, G.S. (Eds.), Sea Ice an Introduction to its Physics, Chemistry, Biology and Geology. Blackwell, Oxford, pp. 333–372.

Armand, L.K., Zielinski, U., 2001. Diatom species of the genus *Rhizosolenia* from Southern Ocean sediments: Distribution and taxonomic notes. Diatom Research 16, 259–294.

Bakker, D.C.E., de Baar, H.J.W., Bathmann, U.V., 1997. Changes of carbon dioxide in surface waters during spring in the Southern Ocean. Deep-Sea Research II 44, 91–127.

Belkin, I.M., Gordon, A.L., 1996. Southern Ocean fronts from the Greenwich meridian to Tasmania. Journal Geophysical Research 101 (C2), 3675–3696.

Broecker, W.S., 2001. The big climate amplifier ocean circulation-sea ice-storminess-dustiness-albedo. In: Seidov, D., Haupt, B.J., Maslin, M. (Eds.), The Oceans and Rapid Climate Change: Past, Present, Future. Geophysical Monograph 126, AGU, Washington, DC, pp. 53–56.

Burckle, L.H., 1983. Diatom dissolution patterns in sediments of the Southern Ocean. Geological Society of American Journal 15, 536–537.

Burckle, L.H., Robinson, D., Cooke, D., 1982. Reappraisal of sea-ice distribution in Atlantic and Pacific sectors of the Southern Ocean at 18 000 yr BP. Nature 299, 435–437.

Climate: Long-Range Investigation, Mapping, and Prediction (CLIMAP) Project Members, 1976. The surface of the Ice Age Earth. Science 191, 1131–1137.

Climate: Long-Range Investigation, Mapping, and Prediction (CLIMAP) Project Members, 1981. Seasonal reconstructions of the Earth's surface at the Last Glacial Maximum. Geological Society of American Map Chart Series MC-36, 1–18.

Comiso, J.C., 2003. Large-scale characteristics and variability of the global sea ice cover. In: Thomas, D.N., Diekmann, G.S. (Eds.), Sea Ice an Introduction to its Physics. Chemistry, Biology and Geology, Blackwell, Oxford, pp. 112–142.

Conkright, M., Levitus, S., O'Brien, T., Boyer, T., J. Antonov, J., Stephens, C., 1998. World Ocean Atlas 1998 CD-ROM Data Set Documentation. National Oceanographic Data Center (NODC) Internal Report, Silver Spring, Maryland, pp. 16.

Cooke, D.W., Hays J.D., 1982. Estimates of Antarctic ocean seasonal ice-cover during glacial intervals. In: Craddock, C. (Ed.), Antarctic Geoscience, IUGS, Ser. B, No. 4, pp. 1017–1025.

Cortese, G., Abelmann, A., 2002. Radiolarian-based paleotemperatures during the last 160 kyr at ODP Site 1089 (Southern Ocean, Atlantic Sector). Palaeogeography, Palaeoclimatology, Palaeoecology 82, 259–286.

Crosta, X., Pichon, J.-J., Burckle, L.H., 1998a. Application of the modern analog technique to marine Antarctic diatoms: reconstruction of maximum sea-ice extent at the Last Glacial Maximum. Paleoceanography 13 (3), 284–297.

Crosta, X., Pichon, J.-J., Burckle, L.H., 1998b. Reappraisal of Antarctic seasonal sea ice at the Last Glacial Maximum. Geophysical Research Letters 25 (14), 2703–2706.

Crosta, X., Sturm, A., Armand, L., Pichon, J.-J., 2004. Late Quaternary sea ice history in the Indian sector of the Southern Ocean as record by diatom assemblages. Marine Micropaleontology 50, 209–223.

Curran, M.A.J., van Ommen, T.D., Morgan, V.I., Philips, K.L., Palmer, A.S., 2003. Ice core evidence for Antarctic sea ice decline since the 1950s. Science 302, 1203–1206.

Dézileau, L., Bareille, G., Reiss, J.L., Lemoine, F., 2000. Evidence for strong sediment redistribution by bottom currents along the southeast Indian Ridge. Deep-Sea Research I 47, 1899–1936.

Drijfhout, S.E., Maier-Reimer, E., Mikolajewicz, U., 1996. Tracing the conveyor belt in the Hamburg large scale geostrophic ocean general circulation model. Journal of Geophysical Research 101, 22563–22575.

Duplessy, J.-C., Labeyrie, L., Waelbroeck, C., 2002. Constraints on the ocean oxygen isotopic enrichment between the Last Glacial Maximum and the Holocene. Paleoceanographic implications. Quaternary Science Reviews 21, 315–330.

Feldberg, M.J., Mix, A.C., 2002. Sea-surface temperature estimates in the Southeast Pacific based on planktonic foraminiferal species: modern calibration and Last Glacial Maximum. Marine Micropaleontology 44, 1–29.

Feldberg, M.J., Mix, A.C., 2003. Planktonic foraminifera, sea surface temperatures, and mechanisms of oceanic change in the Peru and south equatorial currents, 0–150 ka BP. Paleoceanography 18 (1), 1016 doi: 10.1029/2001PA000740.

Fischer, G., Fütterer, D., Gersonde, R., Honjo, S., Ostermann, D., Wefer, G., 1988. Seasonal variability of particle flux in the Weddell Sea and its relation to ice-cover. Nature 335, 426–428.

Fischer, G., Gersonde, R., Wefer, G., 2002. Organic carbon, biogenic silica and diatom fluxes in the Northern Seasonal Ice Zone in the Polar Front Region in the Southern Ocean (Atlantic Sector): Interannual variation and changes in composition. Deep-Sea Research II 49, 1721–1745.

Gersonde, R., Zielinski, U., 2000. The reconstruction of late Quaternary Antarctic sea-ice distribution—The use of diatoms as a proxy for sea-ice. Palaeogeography, Palaeoclimatology, Palaeoecology 162, 263–286.

Gersonde, R., Abelmann, A., Brathauer, U., Becquey, S., Bianchi, C., Cortese, G., Grobe, H., Kuhn, G., Niebler, H.-S., Segl, M., Sieger, R., Zielinski, U., Fütterer, D.K., 2003a. Last glacial sea-surface temperatures and sea-ice extent in the Southern Ocean (Atlantic–Indian sector)—A multiproxy approach. Paleoceanography 18 (3), 1061 doi:1029/2002PA000809.

Gersonde, R., Abelmann, A., Cortese, G., Becquey, S., Bianchi, C., Brathauer, U., Niebler, H.-S., Zielinski, U., Pätzold, J., 2003b. The late Pleistocene South Atlantic and Southern Ocean Surface—A Summary of time-slice and time-series studies. In: Wefer, G., Mulitza, S., Ratmeyer, V. (Eds.), The South Atlantic in the Late Quaternary: Reconstruction of Material Budgets and Current systems. Springer, Berlin, Heidelberg, pp. 499–529.

Gloersen, P., Campbell, W.J., Cavalieri, D.J., Comiso, J.C., Parkinson, C.L., Zwally, H.J., 1992. Arctic and Antarctic sea ice, 1978-1987. Satellite Passive Microwave Observations and Analysis. NASA Special Publication 511, 289 pp., National Aeronautics and Space Administration, Washington, DC.

Gordon, A.L., 1986. Interocean exchange of thermocline water. Journal of Geophysical Research 91, 5037–5046.

Hall, I.R., McCave, N., Shackleton, N.J., Weedon, G., Harris, S.E., 2001. Intensified deep pacific inflow and ventilation in Pleistocene glacial times. Nature 412, 809–812.

Hastie, T., Tibshirani, R., 1990. Generalized Additive Models. Chapman & Hall, London, 335pp.

Hays, J.D., Lozano, J.A., Shackleton, N., Irving, G., 1976. Reconstruction of the Atlantic and western Indian Ocean sectors of the 18 000 B.P. Antarctic Ocean. Geological Society of American Memories 145, 337–372.

Hutson, W.H., 1980. The Agulhas Current during the late Pleistocene: analysis of modern faunal analogs. Science 207, 64–66.

Imbrie, J., Kipp, N.G., 1971. A new micropaleontological method for Quantitative Paleoclimatology: Application to a late Pleistocene Caribbean Core. In: Turekian, K.K. (Ed.), The Late Cenozoic Glacial Ages. Yale University Press, New Haven, Conn., pp. 71–181.

Jöreskog, K.G., Klovan, J.E., Reyment, R.A., 1976. Geological Factor Analysis, Elsevier Science. New York, 178pp.

Keeling, R.F., Stephens, B.B., 2001. Antarctic sea ice and the control of Pleistocene climate instability. Paleoceanography 16, 112–131.

Klinck, J.M., Smith, D.A., 1993. Effect of wind changes during the Last Glacial Maximum on the circulation in the Southern Ocean. Paleoceanography 8, 427–433.

Kucera, M., Rosell-Melé, A., Schneider, R., Waelbroeck, C., Weinelt, M., 2004. Multiproxy Approach for the Reconstruction of the Glacial Ocean surface (MARGO). Quaternary Science Review, this issue, doi:10.1016/j.quascirev.2004.07.017.

Laws, R.A., 1983. Preparing strewn slides for quantitative microscopical analysis: a test using calibrated microspheres. Micropaleontology 24, 60–65.

Le, J., 1992. Palaeotemperature estimation methods: sensitivity test on two western equatorial Pacific cores. Quaternary Science Review 11, 801–820.

Le, J., Shackleton, N.J., 1994. Reconstructing paleoenvironment by transfer function. Model evaluation with simulated data. Marine Micropaleontology 24, 187–199.

Lozano, J.A., Hays, J.D., 1976. Relationship of radiolarian assemblages to sediment types and physical oceanography in the Atlantic and western Indian oceanic sectors of the Antarctic Ocean. In: Cline, R.M., Hays, J.D. (Eds.), Investigations of Late Quaternary Paleoceanography and Paleoclimatology. Geological Society of American Memoirs 145, pp. 303–336.

Mackensen, A., Rudolph, M., Kuhn, G., 2001. Late Pleistocene deep water circulation in the subantarctic eastern Atlantic. Global and Planetary Change 30, 197–229.

Malmgren, B.A., Haq, B.U., 1982. Assessment of quantitative techniques in paleobiogeography. Marine Micropaleontology 7, 213–236.

Matsumoto, K., Lynch-Stieglitz, J., Anderson, R.F., 2001. Similar glacial and Holocene Southern Ocean hydrography. Paleoceanography 16, 445–454.

Maynard, N.G., 1976. Relationship between diatoms in surface sediments of the Atlantic Ocean and the biology and physical oceanography of overlying waters. Paleobiology 2, 99–121.

Mix, A.C., Bard, E., Schneider, R., 2001. Environmental processes of the ice age: land, oceans, glaciers (EPILOG). Quaternary Science Review 20, 627–658.

Moore, K.J., Abbott, M.R., Richman, J.G., 1999. Location and dynamics of the Antarctic Polar Front from satellite sea surface temperature data. Journal Geophysical Research 104 (C2), 3059–3073.

Morales Maqueda, M.A., Rahmstorf, S., 2002. Did Antarctic sea-ice expansion cause glacial CO_2 decline? Geophysical Research Letters 29, 111–113.

Moreno-Ruiz, J.L., Licea, S., 1995. Observations on the valve morphology of *Thalassionema nitzschioides* (Grunow) Hustedt. In: Marino, D., Montresor, M. (Eds.), Proceedings of the 13th International Diatom Symposium. Biopress, Bristol, pp. 393–413.

Naval Oceanography Command Detachment, 1985. In: Sea-ice Climatic Atlas Vol. 1. Antarctic National Space Technology. Lab, Ashville, 131pp.

Niebler, H.-S., Arz, W., Donner, B., Mulitza, S., Pätzold, J., Wefer, G., 2003. Sea-surface temperatures in the equatorial and South Atlantic Ocean during the Last Glacial Maximum (23–19 ka). Paleoceanography 18 (3), 1069 doi: 10.1029/2003PA000902.

Olbers, D., Gouretski, V., Seiß, G., Schröter, J., 1992. Hydrographic Atlas of the Southern Ocean. Alfred Wegener Institute, Bremerhaven, pp. 82.

Pichon, J.-J., Labeyrie, L.D., Bareille, G., Labracherie, M., Duprat, J., Jouzel, J., 1992a. Surface water temperature changes in the high latitudes of the Southern Hemisphere over the Last Glacial–Interglacial cycle. Paleoceanography 7 (3), 289–318.

Pichon, J.-J., Bareille, G., Labracherie, M., Labeyrie, L.D., 1992b. Quantification of the biogenic silica dissolution in the Southern Ocean. Quaternary Research 37, 361–378.

Prell, W.L., 1985. The stability of low-latitude sea-surface temperatures: An evaluation of the CLIMAP reconstruction with emphasis on the positive SST anomalies. Rep. TR 025, pp. 1-60, US Department of Energy, Washington, DC.

Rintoul, S.R., 1991. South Atlantic interbasin exchange. Journal of Geophysical Research 97, 5493–5550.

Sarnthein, M., Gersonde, R., Niebler, S., Pflaumann, U., Spielhagen, R., Thiede, J., Wefer, G., Weinelt, M., 2003. Overview of Glacial Atlantic Ocean Mapping (GLAMAP 2000). Paleoceanography 18 (2), 1030 doi:1029/2002PA000769.

Schlüter, M., Rutgers van der Loeff, M.M., Holby, O., Kuhn, G., 1998. Silica cycle in surface sediments of the South Atlantic. Deep-Sea Research I 45, 1085–1109.

Schrader, H.J., Gersonde, R., 1978. Diatoms and Silicoflagellates. Micropaleontological counting methods and techniques—An exercise on an eight meters section of the lower Pliocene of Capo Rossello. In: Zachariasse, W.J., Riedel, W.R., Sanfilippo, A., Schmidt, R.R., Brolsma, M.J., Schrader, H.J., Gersonde, R., Drooger, M.M., Broekman, J.A. (Eds.), Utrecht Micropaleontological Bulletin 17, 129–176.

Schweitzer, P.N., 1995. Monthly averaged polar sea ice concentration. US Geological Survey Digital Data Series: Virginia. CD, Ed. 1. DDS-27.

Shemesh, A., Burckle, L.H., Hays, J.D., 1995. Late Pleistocene oxygen isotope records of biogenic silica from the Atlantic sector of the Southern Ocean. Paleoceanography 10, 179–196.

Shemesh, A., Hodell, D., Crosta, X., Kanfoush, S., Charles, C., Guilderson, T., 2002. Sequence of events during the last deglaciation in Southern Ocean sediments and Antarctic ice cores. Paleoceanography 17 (4), 1056 doi:10.1029/2000PA000599.

Shin, S.I., Liu, Z., Otto-Bliesner, B.L., Kutzbach, J.E., Vavrus, S., 2003. Southern Ocean control of the glacial North Atlantic thermohaline circulation. Geophysical Research Letters 30 (2), 1096 doi: 10.1029/2002GL015513.

Sieger, R., Gersonde, R., Zielinski, U., 1999. New software package available for quantitative paleoenvironmental reconstructions. EOS 80 (19), 223.

Sigman, D.M., Boyle, E.A., 2000. Glacial/interglacial variations in atmosphere carbon dioxide. Nature 407, 859–869.

Stephens, B.B., Keeling, R.F., 2000. The influence of Antarctic sea ice on glacial–interglacial CO_2 variations. Nature 404, 171–174.

Stocker, T.F., 2003. South dials North. Nature 424, 496–499.

Wolff, E.W., 2003. Whiter Antarctic sea ice? Science 302, 1164.

Wolff, E.W., Rankin, A.M., Röthlisberger, R., 2003. An ice core indicator of Antarctic sea ice productivity? Geophysical Research Letters 30, 2158 doi:10.1029/2003GL018454.

Yokoyama, Y., Lambeck, K., de Dekker, P., Johnson, P., Fifield, K., 2000. Timing for the maximum of the Last Glacial constrained by lowest sea-level observations. Nature 406, 713–716.

Zielinski, U., Gersonde, R., 1997. Diatom distribution in Southern Ocean surface sediments: Implications for paleoenvironmental reconstructions. Palaeogeography, Palaeoclimatology, Palaeoecology 129, 213–250.

Zielinski, U., Gersonde, R., Sieger, R., Fütterer, D.K., 1998. Quaternary surface water temperature estimations—calibration of diatom transfer functions for the Southern Ocean. Paleoceanography 13, 365–383.

Zwally, H.J., Comiso, J.C., Parkinson, C.L., Campbell, W.J., Carsey, F.D., Gloersen, P., 1983. Antarctic Sea Ice 1973–1976: Satellite Passive Microwave Observations. NASA, Washington, DC, Report SP-459.